© 2021. Published by The Company of Biologists Ltd | Development (2021) 148, dev192146. doi:10.1242/dev.192146

RESEARCH ARTICLE

A polarized nucleus-cytoskeleton-ECM connection in migrating cardioblasts controls heart tube formation in *Drosophila*

Cristiana Dondi, Benjamin Bertin, Jean-Philippe Da Ponte, Inga Wojtowicz, Krzysztof Jagla and Guillaume Junion*

ABSTRACT

The formation of the cardiac tube is a remarkable example of complex morphogenetic processes conserved from invertebrates to humans. It involves coordinated collective migration of contralateral rows of cardiac cells. The molecular processes underlying the specification of cardioblasts (CBs) prior to migration are well established and significant advances have been made in understanding the process of lumen formation. However, the mechanisms of collective cardiac cells migration remain elusive. Here, we have identified *CAP* and *MSP300* as novel actors involved during CB migration. They both exhibit highly similar temporal and spatial expression patterns in *Drosophila* migrating cardiac cells, and are necessary for the correct number and alignment of CBs, a prerequisite for the coordination of their collective migration. Our data suggest that CAP and MSP300 are part of a protein complex linking focal adhesion sites to nuclei via the actin cytoskeleton that maintains post-mitotic state and correct alignment of CBs.

KEY WORDS: Cardioblast, Post-mitotic state, Cell alignment, *Drosophila*, Embryogenesis

INTRODUCTION

The genetic network that regulates heart development is highly conserved from flies to humans with orthologous transcription factor (TF) families and signaling pathways essential for heart development, such as Tinman/Nkx2.5, Pannier/GATA4-6, Tailup/Isl1, Dorsocross H15 Mid/Tbx, Hand, Dpp/BMP or Wg/Wnt (Bryantsev and Cripps, 2009; Busser et al., 2015; Jin et al., 2013; Junion et al., 2012; Lovato and Cripps, 2016). However, although mechanistic insights have been gained on the specification of cardiac progenitors, less is known about genes controlling subsequent events of cardiogenesis.

As in mammals, formation of the *Drosophila* heart starts by the migration of bilateral strips of cardiac progenitor cells to the midline and the assembly of a linear heart tube. Cardioblasts (CB) migration occurs concurrently with dorsal closure, a process leading to the spreading of the epidermis dorsally over an extra-embryonic epithelium, the amnioserosa. Migrating CBs extend projections from their dorsal surface and towards the leading edge of the epidermis suggesting coupling of these two tissues (Haack et al., 2014; Rugendorff et al., 1994). However, during the late phase of migration, CBs move cell autonomously. They send out filopodia that contact contralateral CBs and ensure correct cell matching and linear heart tube assembly (Haack et al., 2014; Medioni et al., 2008; Zhang et al., 2018).

Some factors in this process have been identified, including the transmembrane protein Toll (Wang et al., 2005) and Faint sausage, which participates in adhesion between ipsilateral CBs (Haag et al., 1999).

Proteins involved in setting or maintaining polarity of CBs have also been implicated in collective migration. Among them, the integrin dimer expressed by the CBs (αPS3 and βPS), its ligand Laminin-A and cytoplasmic integrin adapter Talin are all required for proper CBs alignment (Stark et al., 1997; Vanderploeg and Jacobs, 2015; Vanderploeg et al., 2012).

Moreover, the coordinated migration and alignment of CBs requires the Slit morphogen and its receptor Robo (MacMullin and Jacobs, 2006; Qian et al., 2005). Slit function in cardiac cell migration is conserved from *Drosophila* to vertebrates. In zebrafish, Slit2 knockdown embryos show disruption of endocardial collective cell migration, with individual cells migrating faster and with loss of directionality (Fish et al., 2011).

Recent findings have shown a genetic interaction between αPS3 gene *scb* and *Slit/Robo*, suggesting an integrated function of cell membrane-associated factors in CB migration polarization during cardiac tube formation (Vanderploeg et al., 2012). The link between cell adhesion and actin cytoskeleton remodeling is also fundamental for CB migration and requires intermediate proteins to mediate connections and to transduce signals. Among them, two members of the Dock Guanine nucleotide Exchange Factors (GEFs) containing SH3 domain, Myoblast city and Sponge, are required during CB migration through activation of Rac and Rap1, respectively (Biersmith et al., 2015). Mutants for these two genes have defects in the migrating CB rows, with gaps and clusters of multilayered CBs. Moreover, the Rho GTPase CDC42 is required in Tinman-positive CBs for the contact with the opposite row (Swope et al., 2014; Vogler et al., 2014) by modulating localization of non-muscle myosin II Zipper (Vogler et al., 2014). Thus, cytoskeleton modulations allow filopodia formation at the CBs leading edge and ensure coordinated, tension-mediated modification of cell shape to keep migrating CBs aligned.

Here, we identify the SORBS Cbl Associated Protein (CAP) and Muscle Specific Protein 300 (MSP300, also known as Msp300) as novel mediators of the transition from mitotic state to CBs migration. *In vitro*, SORBS proteins are generally targeted to focal adhesion sites, where they play diverse roles in mechano-transduction, contributing to stiffness sensing and contractility (Ichikawa et al., 2017). CAP is the only SORBS family member in *Drosophila* and has been described as an adaptor protein that makes links between different partners at the membrane-cytoskeletal

Université Clermont Auvergne, CNRS 6293, Inserm 1103, GReD institute, F-63000 Clermont-Ferrand, France.

*Author for correspondence (guillaume.junion@uca.fr)

I.W., 0000-0002-2746-2163; G.J., 0000-0003-0458-6021

Handling Editor: Benoit Bruneau
Received 30 April 2020; Accepted 29 June 2021

Development (2021) 148, dev192146. doi:10.1242/dev.192146

interface of stretch-sensitive structures via the vinculin-integrin complex (Bharadwaj et al., 2013).

MSP300 is a large protein of the Nesprin family with several protein domains, including spectrin and nuclear anchoring KASH domains. Nesprin provides a link between actin cytoskeleton and perinuclear layer via Linker of Nucleoskeleton and Cytoskeleton (LINC) (Mellad et al., 2011). Recently, MSP300 has been shown to display stretching capacity participating in the elasticity of a myonuclear scaffold to protect myonuclei from mechanical stress (Wang et al., 2015).

Nucleus deformability is necessary when cells are squeezing through small constrictions during their migration (Friedl et al., 2011). The role of the nucleus in cell migration is suggested to be dependent on its connections with components of the cytoskeleton mediated by LINC and indirectly with extracellular matrix, including focal adhesion complex (Fruleux and Hawkins, 2016).

In the developing heart, our data show that CAP and MSP300 accumulate in a punctate manner on apical and basal sides of migrating CBs. We also demonstrate that polarized accumulation of nuclei-anchored MSP300 and cell membrane associated CAP promote post-mitotic state and are required for CB alignment, coordinated migration and proper CB nuclei shapes. These findings imply the requirement of polarized nucleus-cytoskeleton-ECM connections during collective CB migration.

RESULTS

CAP and MSP300 accumulate interdependently in apical and basal dots in migrating cardioblasts

Because coordinated CB migration towards the midline involves stretch-induced morphological changes of cells, we asked whether CAP and MSP300 could be involved in these processes as their functions have not yet been investigated in *Drosophila* heart. Orthologous genes, SORBS family and *Syne1*, respectively, exhibit

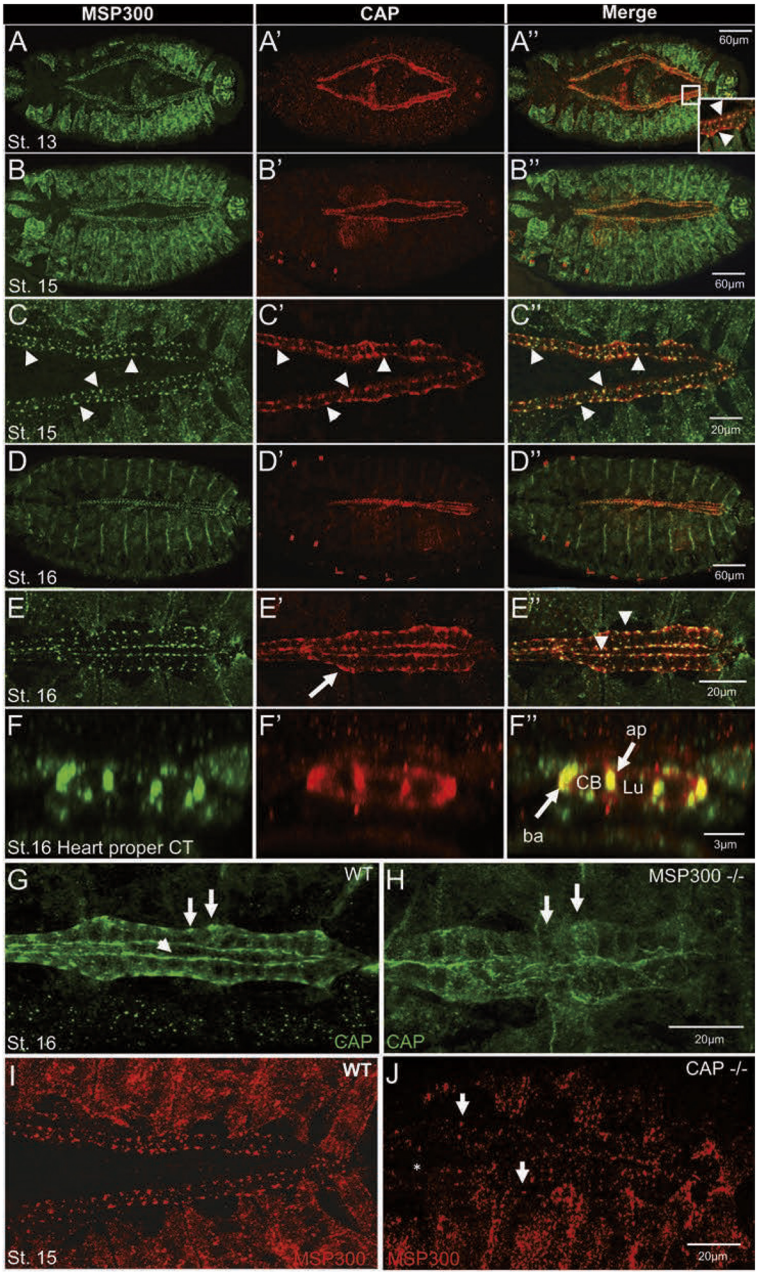

Fig. 1. CAP and MSP300 colocalize in CBs in basal and apical dots inter-dependently. (A-A″) Dorsal view of a late stage 13 embryo immunostained using anti-CAP and anti-MSP300 antibodies showing co-expression in cardioblasts. Inset in A″ indicates the boxed region showing colocalization of CAP and MSP300 at both sides of migrating cardioblasts (arrowheads). (B-B″) Dorsal view of an early stage 15 embryo showing that CAP and MSP300 accumulate in dots on the basal and apical sides of cardioblasts. (C-C″) Higher magnification showing that MSP300 accumulates where CAP proteins are at their highest levels on apical and basal sides (arrowheads). (D-D″) Dorsal view of a stage 16 embryo showing that the CAP and MSP300 punctate expression pattern is present until the stage of lumen formation. We also observed a colocalization in muscle attachment sites at segmental borders. (E-E″) Higher magnification showing that CAP accumulation is extended under the cell membrane (arrow), and that CAP and MSP300 colocalize on basal and luminal sides (arrowheads). (F-F″) 3D reconstruction of a transverse cut in the heart proper that confirms accumulation of MSP300 and CAP on basal and apical sides of CBs (arrows) (ba, basal side; ap, apical side; Lu, lumen; CB, cardioblast). (G,H) Dorsal view of a stage 16 embryo showing that loss of MSP300 induces a strong decrease in CAP localization on basal (arrows) and apical (arrowhead) sides. (I,J) Dorsal view of a stage 15 embryo showing that loss of CAP leads to a partial reduction in the punctate pattern of MSP300 localization. Some dots are still visible in a few CBs (arrows).

Development (2021) 148, dev192146. doi:10.1242/dev.192146

conserved cardiac expression in mammals (Banerjee et al., 2014; Dixon et al., 2015; Hong et al., 2014; Puckelwartz et al., 2010).

We first tested expression patterns of CAP and MSP300 by immunostaining and confirmed that they are both expressed in migrating CBs, starting from late embryonic stage 13 (Fig. 1A-A″). CAP and MSP300 are co-expressed in a stereotyped punctate pattern on the apical and basal sides of each CB, clearly visible from stage 15 (Fig. 1B-B″ and arrowheads in Fig. 1C-C″). This expression is maintained when the two rows of CBs have reached the dorsal midline (Fig. 1D-E″). Although expression of CAP seems to be also diffuse under cell membranes (arrow in Fig. 1E′), MSP300 is largely colocalized with CAP protein (arrowheads in Fig. 1E″). Transverse sections of 3D reconstructed developing hearts confirmed colocalization of CAP and MSP300 on basal and apical sides of CBs in aorta, as well as in the heart proper (arrows in Fig. 1F-F″, Fig. S1A,B). To validate CAP and MSP300 localization in the apical side of the luminal domain, we performed co-immunostaining experiments with CAP and Slit antibodies (Fig. S1C-F″). We confirmed that CAP and MSP300 are enriched apically at the level of the lumen (arrowheads in Fig. S1C-E) but absent at the CB adhesion sites characterized by Armadillo expression (Fig. S1G,H). Unexpectedly, we also observed Slit localization in a punctate pattern at the basal side of CBs at stage 15-16, reminiscent of CAP and MSP300 expression patterns (arrows in Fig. S1C-C″). This dotty accumulation of Slit is transient as it becomes polarized at the luminal side at late stage 16 (Fig. S1F-F″).

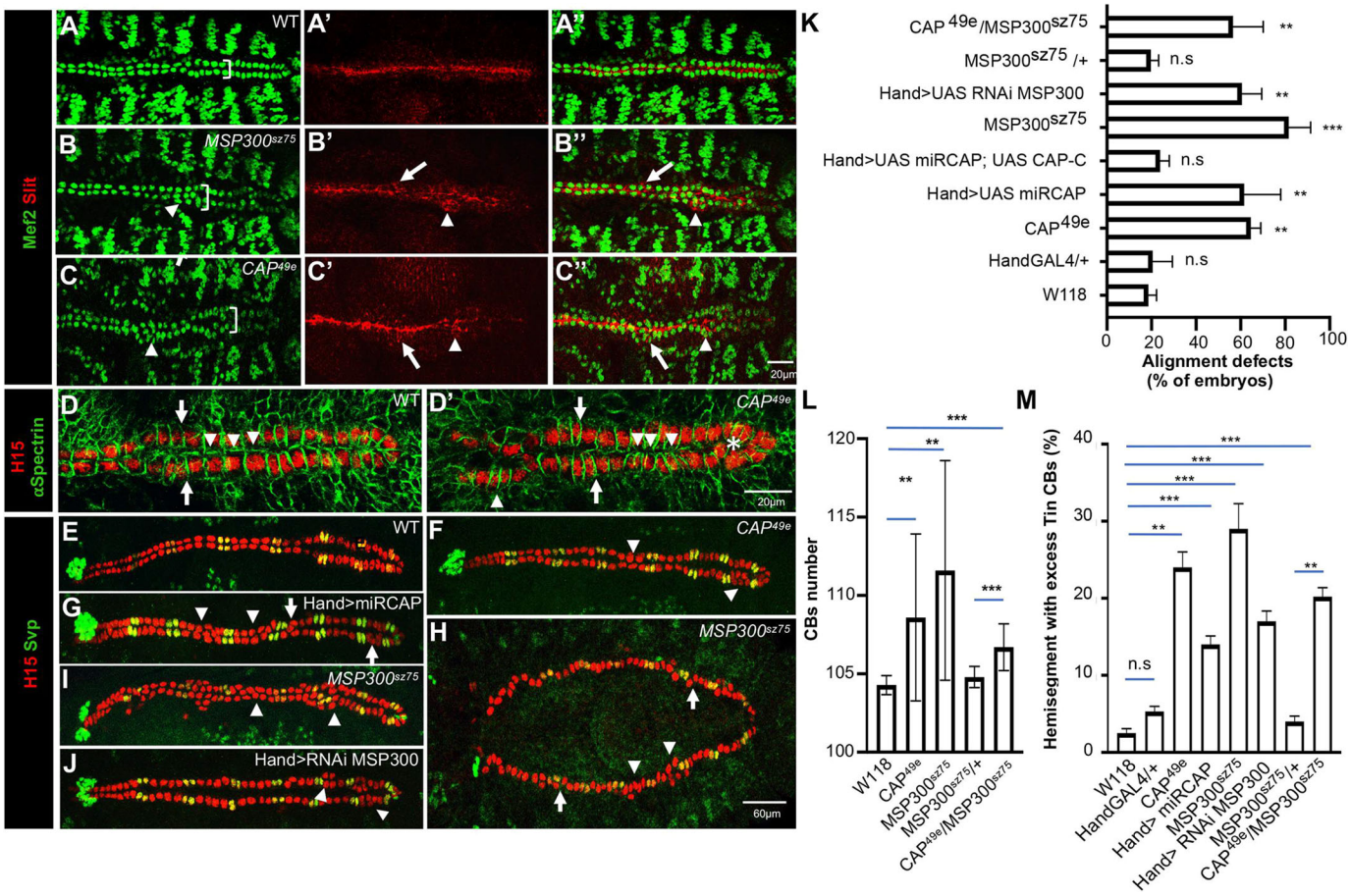

Fig. 2. MSP300 and CAP are required for correct CB alignment and number during migration. (A-C″) Dorsal view of stage 16 embryos showing that, compared with wild type, the loss of MSP300 and CAP induces alignment defects visible using the CB nuclear marker Mef2 and the CB polarity marker Slit. (A-A″) The wild-type equivalent with two rows of CBs (bracket) and apically localized Slit protein. (B-B″) After loss of *MSP300*, more than two rows of CBs are visible in some segments (bracket) and the Slit pattern is not polarized, with some accumulation visible on lateral and basal side of CBs. Arrowhead and arrows indicate ectopic accumulation of Slit on basal and lateral side of CBs, respectively. (C-C″) *CAP49e* mutant embryos show similar phenotypes to the loss of *MSP300*. (D,D′) The cell membrane marker α-Spectrin shows that, in the *CAP49e* mutant, cells are misaligned and pairing between contralateral CBs is disturbed (compare arrows in D and D′). This impacts contacts between CBs (compare arrowheads in D and D′). Mislocalized cells are also visible in *CAP* mutant (asterisk). (E-G,I,J) Dorsal view of stage 16 embryos specifically revealing (using anti-H15 antibody) all the cardiomyocytes, including Svp-positive ostia cells (stained using an anti-Svp antibody). *CAP49e* and *MSP300sz75* homozygous mutants, as well as cardiac-specific knockdown of these two genes, have an increase in the number of Tin-positive CBs in some hemi-segments (arrowheads). The number of Svp-positive CBs remains unchanged. Arrows indicate hemi-segments with correct CB number but bearing alignment defects. (H) Dorsal view of a stage 14 embryo revealing uncoordinated CB migration in *MSP300sz75* homozygous mutants in hemi-segments with (arrowheads) or without (arrows) an increase in the number of Tin-positive CBs. (K) Bar chart showing the percentage of embryos with CB alignment defects (CAP49e *n*=52, MSP300 *n*=55, all other genotypes *n*=30). Data are mean±s.d. Two-tailed *P*-values were calculated using a Wilcoxon-Mann-Whitney test, ***P*<0.001, ****P*<0.0001. (L) Bar chart showing quantification of mean number of CBs in the indicated genetic backgrounds (*n*=30). Data are mean±s.d. Two-tailed *P*-values were calculated using a Wilcoxon-Mann-Whitney test, ***P*<0.001, ****P*<0.0001. (M) Bar chart showing the percentage of hemi-segments with supernumerary Tin-positive CBs (W118 *n*=240, *CAP49e* *n*=360, Hand>miRCAP *n*=240, *MSP300sz75* *n*=360, Hand>RNAi MSP300 *n*=240, *MSP300sz75*/+ *n*=240 and *MSP300sz75*/*CAP49e* *n*=240). Data are mean±s.d. Two-tailed *P* were calculated using a Wilcoxon-Mann-Whitney test, ***P*<0.001, ****P*<0.0001.

Development (2021) 148, dev192146. doi:10.1242/dev.192146

Next, we wondered whether the punctate localizations of CAP and MSP300 are interdependent. MSP300 is a multidomain scaffold protein. Therefore, we hypothesized that it could participate in the recruitment and accumulation of CAP into subcellular compartments, creating a repeated punctate pattern. To test this, we performed immunostaining in both CAP and MSP300 mutants. We observed a clear loss of punctate accumulation of CAP on basal and apical CB sides in *MSP300*^{SZ75} mutant embryos, suggesting that MSP300 is required for CAP localization in CBs (arrows, Fig. 1G,H). Similarly, in *dCAP49e* mutants (in which a 2.9 kb region downstream of the CAP^{CA06924} P-element is deleted), the MSP300 expression pattern is severely affected. However, as some MSP300 expression in CBs persists, we conclude that CAP is only partially required for the MSP300 punctate pattern (arrows, Fig. 1I,J). We also performed co-immunoprecipitation experiments using GFP-tagged MSP300 transgenic *Drosophila* line but could not find any interaction between MSP300-GFP and CAP under our experimental conditions, indicating that several intermediate partners might be involved in the complex.

In summary, we observed that during the late phase of CBs migration, CAP, MSP300 and Slit colocalize in polarized dots on each side of the CBs in the basal and luminal domains. These findings suggest that CAP and MSP300 are part of a protein complex as their punctate localization appears to be largely interdependent.

MSP300 and CAP are required for the correct alignment and number of Tin+ cardioblasts

We next examined *CAP* and *MSP300* functions during CB migration. Immunostaining with antibodies against the muscle differentiation transcription factor Mef2 revealed misalignments of CBs in both *MSP300* and *CAP* mutants (Fig. 2A-C″). Cardioblasts formed clusters (arrowheads in Fig. 2B,C) and multiple cell layers (brackets, Fig. 2B,C). We scored these alignment defects and found that 80% of *MSP300* (44/55) and 64% of *CAP* mutant embryos (34/52) present a multilayered row of CBs, suggesting that *MSP300* and *CAP* are both involved in maintaining cohesion of migrating CBs (Fig. 2K).

Slit and its Robo receptors are known factors in CB migration, alignment and polarization (MacMullin and Jacobs, 2006; Medioni et al., 2008; Qian et al., 2005; Santiago-Martinez et al., 2006). Slit- and Robo-mediated cardiac morphogenesis is modulated by the transmembrane integrin receptors, their ligands and intracellular interactors (Vanderploeg et al., 2012). Given the link between CAP and the integrin adhesion complex, as well as the observed alignment defects in *dCAP49e* embryos, we tested whether Slit localization is affected in *CAP* and *MSP300* mutants.

We found clear Slit localization defects in both mutants. (Fig. 2A-C″). Slit was ectopically expressed in misaligned CBs, creating a meshwork between CBs (arrows in Fig. 2B′,C′). Similar ectopic enrichment of Slit around mislocalized CBs has also been observed in cardiac-specific knockdowns of *CAP* (miR strategy; Bharadwaj et al., 2013) and *MSP300* (short hairpin mediated strategy) (Fig. 2K, Fig. S2A-B″). Collectively, these data show that CAP and MSP300 ensure correct Slit localization in CBs. They also suggest a potential interaction between CAP, MSP300 and the integrin complex in migrating CBs.

We then tested whether the CB cell shape is affected in *CAP* mutants. α-Spectrin staining, which marks cell membrane subdomain, showed that *CAP*^{49e} CBs are misarranged compared

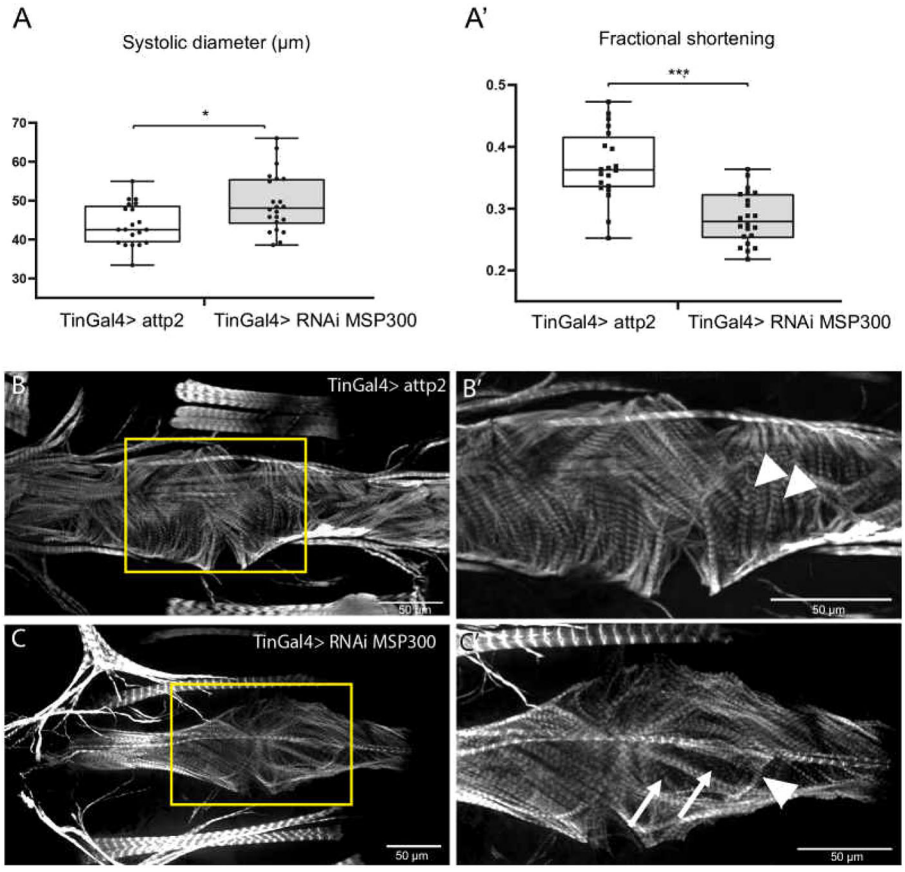

Fig. 3. Cardiac-specific MSP300 knockdown causes a reduction in contractility and myofibrillar disorganization. (A,A′) Contractility is impaired in MSP300 knockdown hearts from 3-week-old female flies that show an increased systolic diameter (A) and reduced fractional shortening (A′) (control *n*=20; MSP300 RNAi *n*=22). Data analysis using a Wilcoxon-Mann-Whitney test demonstrates that the difference between controls and MSP300 RNAi is statistically significant (**P*<0.05, ****P*<0.0001). The values of the box represent first and third quartile and the line represents the median. The whiskers represent the minimum and maximum of all the data. (B) Control heart stained for F-actin showing highly organized and densely packed circumferential myofibers. (B′) Higher magnification view of a control heart with dense cardiomyocytes fibers (arrowheads). (C) An MSP300 knockdown heart shows high disorganization of the myofibers and gaps between them. (C′) Higher magnification view of an MSP300 knockdown heart showing the lack of fibers compared with control (arrowhead) leading to gaps (arrows) between cardiomyocyte myofibers. Scale bars: 50 µm.

Development (2021) 148, dev192146. doi:10.1242/dev.192146

with the wild type (where CBs are perfectly aligned along AP axis and matching with their contralateral partner) (arrows and arrowheads in Fig. 2D). In *CAP*^{49e} hearts, we observed changes in both the shapes and the orientation of CBs along the A-P axis (arrowhead in Fig. 2D′), CB misalignment/matching defects (arrows and arrowheads, Fig. 2D,D′) and mispositioning within rows of cells (star in Fig. 2D′), suggesting mis-regulation of CB migration directionality.

We also tested the genetic interaction between *CAP* and *MSP300* using trans-heterozygous *dCAP49e/MSP300*^{SZ75} mutant embryos. In contrast to the single heterozygous control, CB alignment is affected in trans-heterozygotes (18% versus 59%; Fig. 2K, Fig. S2C-C″), showing that *CAP* and *MSP300* genetically interact and play convergent roles during CB migration. Finally, we checked whether changes in total cardiac cells number could account for *MSP300* and *CAP* mutant phenotypes. We performed immunostaining experiments using antibodies against H15, a transcription factor specific to all CBs, and Seven-up (Svp), a marker of a CB subset that gives rise to ostia. These two markers allow the four Tin-positive CBs (Svp negative) to be distinguished from the two Svp-positive CBs in each abdominal hemi-segment A2-A7. We found that knockout of either *MSP300* or *CAP* both led to a significant increase in CB number (Fig. 2E-J,L). Interestingly, only Tin-positive CB levels were increased in homozygous mutant or cardiac-specific knockdowns of either *CAP* or *MSP300*, suggesting a specific function of these genes in maintaining the post-mitotic state of Tin^{+} CBs (Fig. 2E-J,M, Fig. S5) thought to undergo symmetric cell divisions. Alignment defects also occur in hemi-segments without supernumerary CBs, but this appears to be concomitant with an increase in CBs in other hemi-segments. (arrows in Fig. 2G,H).

MSP300 is required for proper adult heart structure and function

Considering the impact of MSP300 loss of function on embryonic heart morphology and that MSP300^{sz75} homozygous mutants are embryonic lethal, we wondered whether cardiac-specific knockdown of MSP300 could lead to some defects in the adult heart. We first validated the efficiency of an MSP300 RNAi line in embryos by immunostaining (Fig. S3A-B′) and analyzed

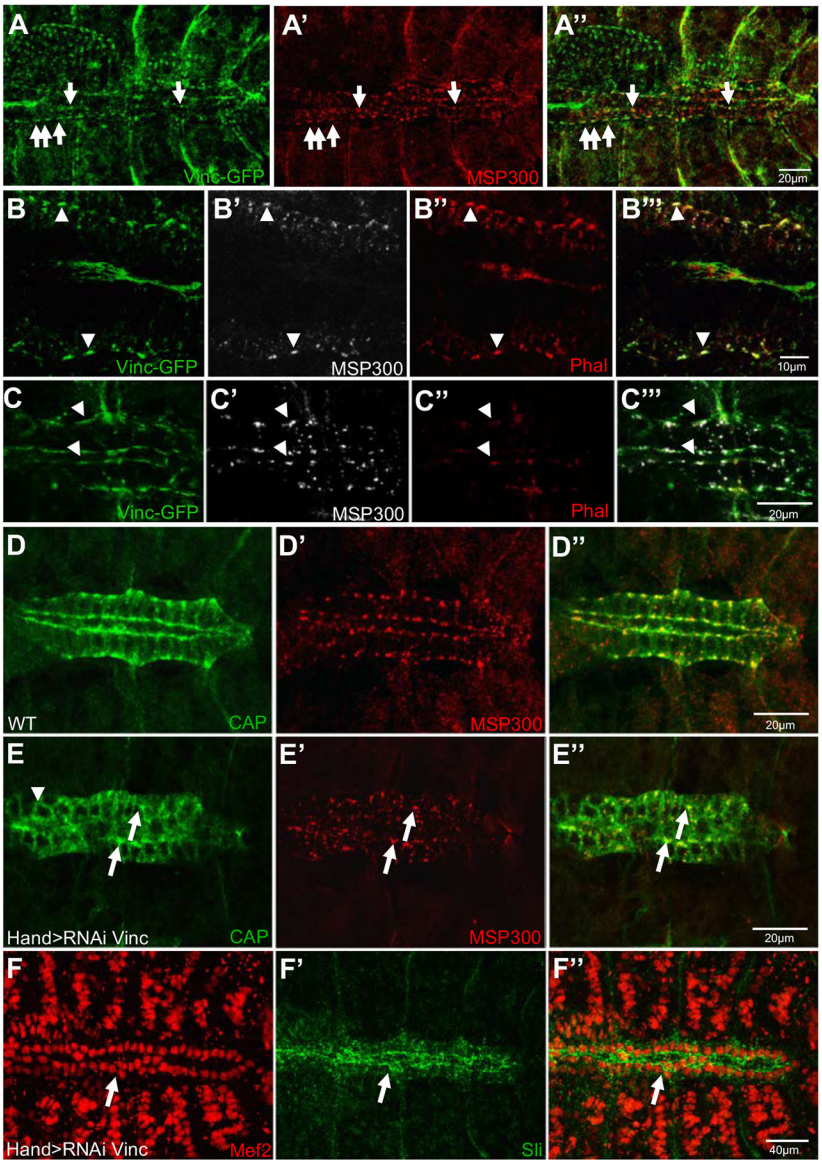

Fig. 4. Vinculin controls polarized accumulation of CAP and MSP300 in CBs. (A-A″) Dorsal view of stage 16 embryos revealing Vinculin-GFP localization in a spotty pattern in close proximity to MSP300 accumulation on basal and apical sides (arrows). (B-B‴) Higher magnification images showing that MSP300 accumulates where Vinc-GFP levels are highest. Here, the pictures are focused on the basal side of CBs. The Vinculin partner F-actin is also present in a similar dotty pattern (B″,B‴). Arrowheads indicate colocalization on the basal side of CBs. (C-C‴) Higher magnifications showing that Vinculin is present at a similar level on the apical side of CBs. Arrowheads indicate colocalization on apical and basal sides. (D-E″) Immunostaining with anti-CAP and anti-MSP300 antibodies in wild type (D-D″), and cardiac-specific *Vinculin* knockdown (E-E″). Accumulation of CAP and MSP300 is still visible but in a disorganized pattern (arrows), suggesting polarity defects and leading to mislocalization of CBs (arrowhead in E). (F-F″) *Hand>RNAi-Vinc* leads to mislocalization of CBs and affects polarized localization of Slit. Arrowheads indicate ectopic accumulation of Slit between CBs arranged as a cluster.

Development (2021) 148, dev192146. doi:10.1242/dev.192146

semi-intact preparations of the fly hearts to measure heart physiological parameters after knockdown using SOHA software (Ocorr et al., 2007).

MSP300 RNAi flies show a significant increase in systolic diameter leading to a reduction in fractional shortening (Fig. 3A,A′). MSP300 RNAi hearts stained for F-actin also show disorganization and gaps (arrows in Fig. 3C′) in the circumferential myofibrils in comparison with highly organized and densely packed myofibrils observed in control hearts (arrowheads in Fig. 3B′-C′). This disturbed cardiac architecture suggests a potential discontinuity in the arrangement of cardiomyocytes, leading to failure in coordinated contraction.

The Vinculin-β-Integrin complex is required for CAP and MSP300 polarized localization

CAP protein interacts directly with Vinculin (Vinc) at the muscle attachment sites, where it is recruited to the integrin complex to modulate the Actin cytoskeleton (Bharadwaj et al., 2013). Therefore, we asked whether Vinc is also present in CBs during embryonic development and could be involved in CAP-regulated processes. We took advantage of a recently generated Vinc-GFP knock-in allele allowing us to follow Vinc localization *in vivo*. We detected restricted and similar Vinc-GFP signal at the apical and basal membranes of CBs, consistent with CAP and MSP300 expression (arrows, Fig. 4A-B‴) as well as the localization of other integrin adhesion complex members, such as βPS-Integrin (Myospheroid) (arrows, Fig. S4A-A″). Interestingly, we confirmed that this accumulation of Vinc coincides with F-actin localization at basal (arrowheads, Fig. 4B-B‴) and apical sides, revealed with Phalloidin staining (arrowheads, Fig. 4C-C‴, Fig. S4B-B‴).

To test whether Vinc is required for CAP localization, we analyzed the impact of heart-specific *Vinc* knockdown on both CAP and MSP300 expression (Fig. 4D-E″). We first validated the

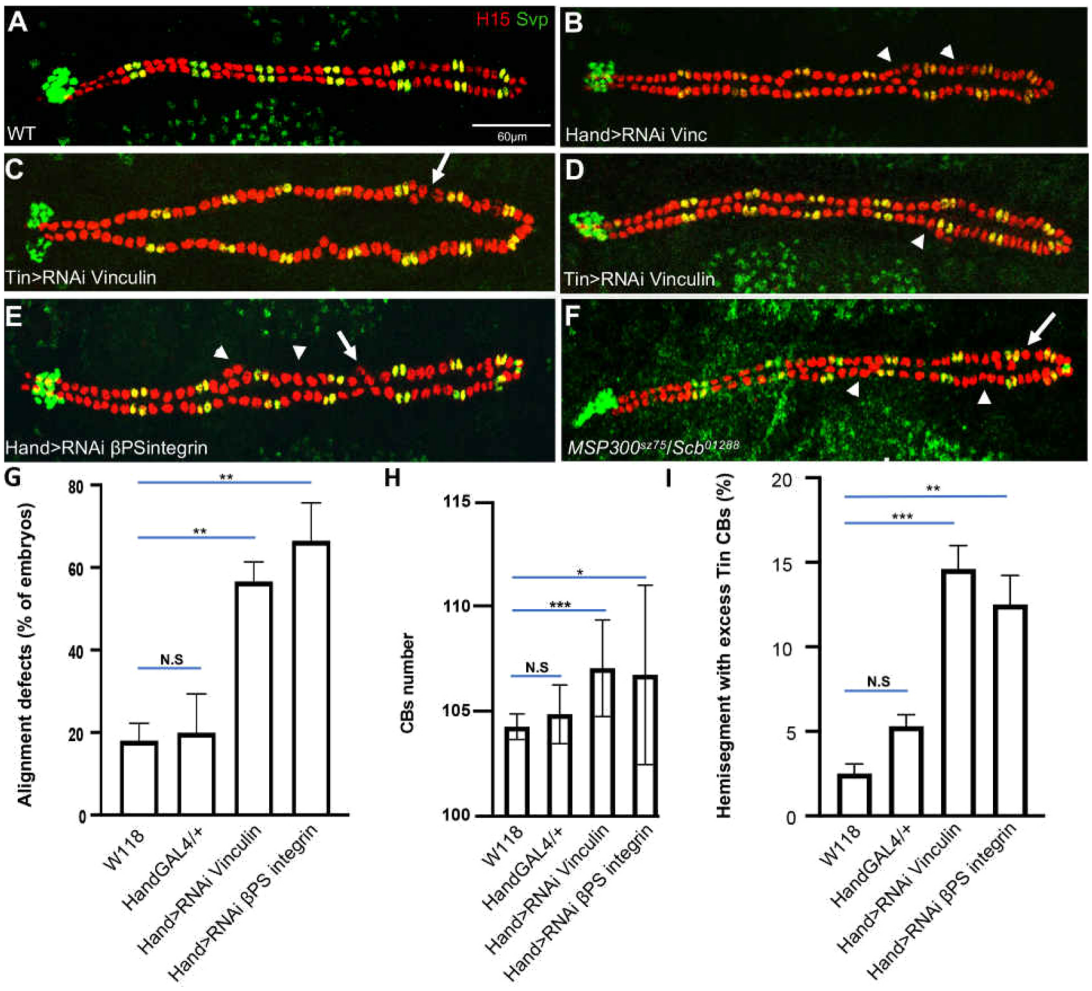

Fig. 5. The Vinculin/integrin complex regulates CB alignment and number. (A,B) Compared with wild type, *Hand>RNAi-Vinc* induces a specific increase in Tin-positive CBs in two hemi-segments (arrowheads). (C,D) Inducible knockdown of Vinculin with a Tin-Gal4 driver leads to alignment defects (arrow) and an increase in Tin-positive CBs (arrowhead) in some cardiac cell hemi-segments during migration, leading to cardiac tube misalignment. (E) Inducible knockdown of βPS Integrin with a Hand-GAL4 driver leads to misalignment of CBs (arrow) and an increase in Tin-positive CBs in some cardiac cell hemi-segments (arrowheads). (F) A double heterozygous embryo with mutations in *MSP300* and αPS3 integrin shows similar defects of misalignment (arrows) and an increase in Tin-positive CBs (arrowheads), suggesting a genetic interaction. (G) Bar chart showing the percentage of embryos with CB alignment defects (n=30). Data are mean±s.d. Two-tailed P-values were calculated using a Wilcoxon-Mann-Whitney test, $^{**}P<0.01$, $^{***}P<0.0001$. (H) Bar chart showing quantification of the mean CB number in the indicated genetic backgrounds (n=30). Data are mean±s.d. Two-tailed P-values were calculated using a Wilcoxon-Mann-Whitney test, $^{*}P<0.05$, $^{***}P<0.0001$. (I) Bar chart showing the percentage of hemi-segments with excess Tin-positive CBs (n=240). Data are mean±s.d. Two-tailed P-values were calculated using a Wilcoxon-Mann-Whitney test, $^{**}P<0.01$, $^{***}P<0.0001$.

Development (2021) 148, dev192146. doi:10.1242/dev.192146

efficiency of *Vinc* knockdown by immunostaining in embryos (Fig. S3C-D′) and observed that the heart proper morphology contains inclusion of CBs (Fig. 4E, arrowhead) indicating their misalignment during migration. Dots of co-accumulation of CAP and MSP300 are still present; however, their pattern is disorganized, suggesting that polarization of CBs is defective (arrows, Fig. 4E-E″). Cardiac-specific knockdown of *Vinc* also induces a meshwork of Slit (Fig. 4F-F″) and an increase in Tin-positive CBs in some hemi-segments, which is consistent with CAP and MSP300 loss of function (Fig. 5A-D,G-I). Similar results are also obtained by cardiac-specific knockdown of βPS-Integrin (*mys*) (Fig. 5E,G-I). Interestingly, transheterozygous mutant embryos with *MSP300sz75* combined with the cardiac α-PS3-Integrin mutation scb^{01288} show disorganized CB alignment and an increased number of Tin-positive CBs (Fig. 5F), showing their involvement in the same pathway. These results are reminiscent of the genetic interaction recently identified between *CAP* and *scb* (Jammrath et al., 2020), suggesting related roles of CAP, MSP300 and the integrin complex in controlling the postmitotic state of Tin-positive CBs. Finally, we tested whether the integrin ligand Laminin A (LamA), which is also known to interact genetically with *slit* (MacMullin and Jacobs, 2006), is affected by the loss of *MSP300*, *Vinc* and βPS-integrin. Interestingly, we observed a disorganized pattern of LamA in *MSP300* homozygous mutant embryos with breaks in the apical side and the basal lamina, suggesting that Nesprin-like proteins are required for ECM structure (Fig. 6A-B′). These results are consistent with defects in LamA pattern observed after *Vinc* and βPS-integrin knockdown (Fig. 6A″-B‴). A similar requirement for MSP300 and the integrin complex was also observed for the correct localization of another ECM component Perlecan (Trol), a secreted heparan sulfate proteoglycan (Fig. 6C-D‴). Overall, the polarized location of the CAP-MSP300-Vinc/integrin complexes plays an important role in determining the appropriate number and arrangement of CBs, and the localization of ECM proteins.

CAP and MSP300 mediate F-actin bridging between the nucleus and integrin complex

CAP and MSP300 might function by locally binding Vinc adhesion complexes to the actin cytoskeleton and the nucleus. This would generate a directional internal tension that would keep the CBs polarized, maintain their postmitotic state and their alignment, and thus allow correct lumen formation and compaction of the heart tube. MSP300/Syne 1-2 proteins contain an actin-binding domain, whereas CAP binds to actin-binding proteins, including Vinc. This suggests that F-actin might be a potential co-partner associated to the MSP300-CAP-Vinc dots during CB migration. To confirm the involvement of F-actin in bridging the nucleus to the integrin complex, we analyzed null mutation and cardiac-specific KD of WASp. WASp regulates the nucleation activity of the Arp2/3 complex, facilitating the assembly of branched actin filament networks with the spatiotemporal control required to orchestrate cellular processes (Padrick et al., 2011).

Consistent with our previous findings, cardiac (Hand-GAL4) or Tin-positive CBs with specific knockdown of WASp have defects in alignment of cardiac cells and an increased number of Tin-positive CBs in some hemi-segments (Fig. 7A-D,F-H and Fig. S5). These defective arrangements of CBs also occur in hemi-segments bearing the correct number of Tin CBs (arrows in Fig. 7D), suggesting that clustering could occur as a consequence of exiting the post-mitotic state of CBs in a different hemi-segment. Finally, we assessed the genetic interaction between *MSP300* and *WASP* by comparing single heterozygous mutant for each gene with the transheterozygous mutant. Our results clearly demonstrate a

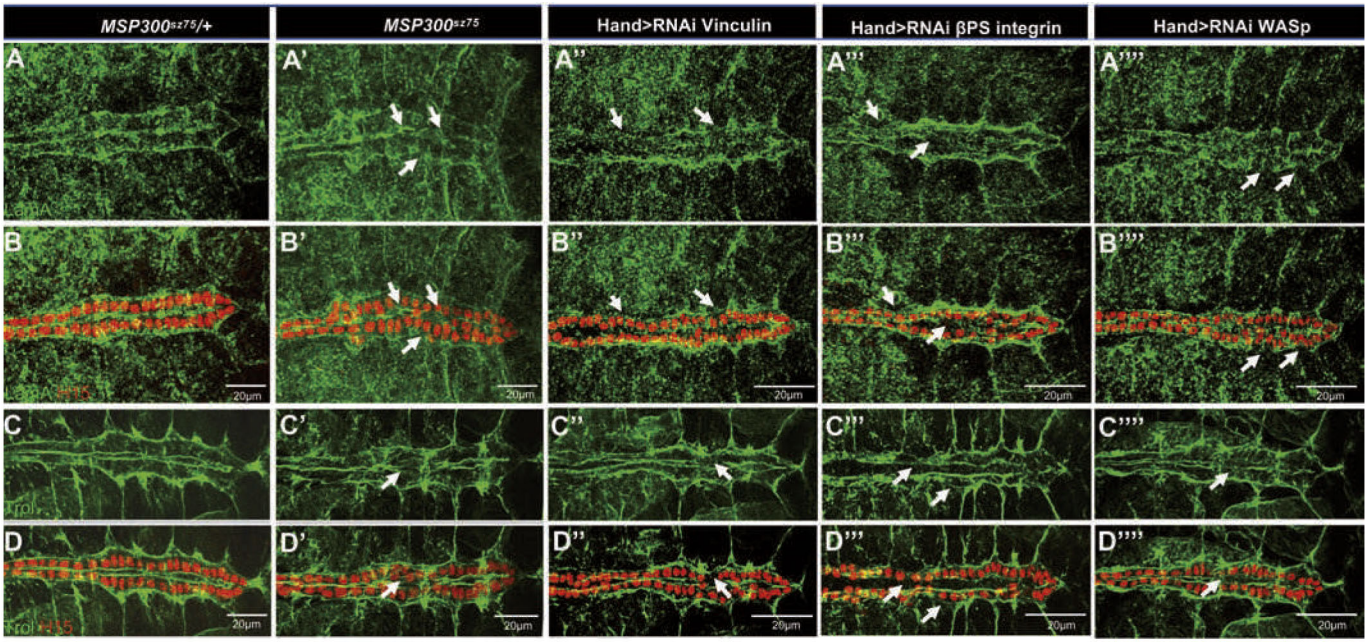

Fig. 6. The localization of the ECM proteins Laminin A and Trol is affected by MSP300, Vinculin/Integrin and WASp loss of function. (A,A′,B,B′) Immunostaining showing that loss of MSP300 induces a disorganized pattern of Laminin A on basal and apical sides of CBs. The LamA-positive basal layer is thinner and holes are visible around some mispositioned CBs (arrows) stained using anti-H15 antibody. (C,C′,D,D′) Immunostaining showing that loss of MSP300 leads to a defect in Perlecan (Trol) localization around disorganized CBs (arrow). Anti-H15 antibodies are used to stain CBs. (A″,B″,C″,D″) Cardiac-specific knockdown of Vinc leads to defects in LamA and Trol localization around misaligned CBs. Arrows indicate a discontinuous layer of ECM compared with control. (A‴,B‴,C‴,D‴) Similar results were obtained after cardiac-specific knockdown of βPS integrin. (A⁗,B⁗,C⁗,D⁗) Downregulating the branched actin regulator WASp in cardiac cells leads to a disorganized pattern of expression of the ECM proteins LamA and Trol (arrows).

Development (2021) 148, dev192146. doi:10.1242/dev.192146

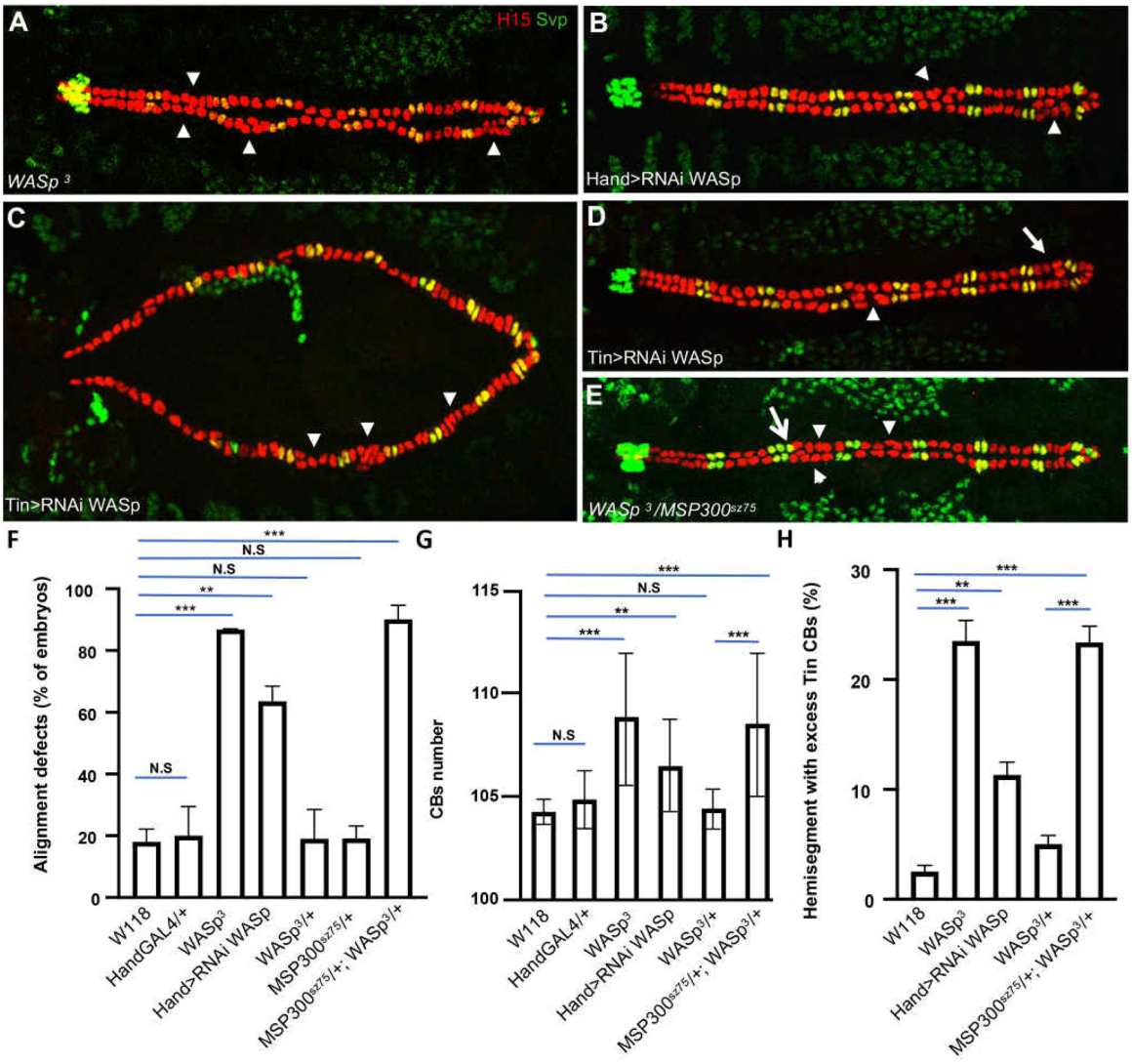

Fig. 7. The Arp2/3 complex activator *WASp* interacts genetically with *MSP300* during CB migration. (A) A *WASp*^{3} homozygous mutant embryo showing excess Tin-positive CBs in several hemi-segments (arrowheads) and closure defects. (B) Inducible knockdown of WASp with a Hand-GAL4 driver leads to misalignment of CBs and an increase in Tin-positive CBs in some cardiac cell hemi-segments (arrowheads). (C,D) Similar defects are observed from stage 14 with a Tin-positive CB-specific driver. Arrowheads in C,D indicate the increased number of Tin-positive CBs and the arrow in D indicates misalignment without a change in the number of Tin-positive CBs. (E) A *WASp*^{3} and *MSP300*^{sz75} transheterozygous mutant embryo showing an increased number of Tin-positive CBs (arrowheads) leading to alignment defects suggesting genetic interaction. At lower frequency additional Svp-positive CBs are also visible (arrow). (F) Bar chart showing the percentage of embryos with CB alignment defects (n=40). Data are mean±s.d. Two-tailed P-values were calculated using a Wilcoxon-Mann-Whitney test, **P<0.01, ***P<0.0001. (G) Bar chart showing quantification of the mean number of CBs in the indicated genetic backgrounds (n=30). Data are mean±s.d. Two-tailed P vales were calculated using a Wilcoxon-Mann-Whitney test, **P<0.01, ***P<0.0001. (H) Bar chart showing the percentage of hemi-segments with excess Tin-positive CBs (n=240). Data are mean±s.d. Two-tailed P-values were calculated using a Wilcoxon-Mann-Whitney test, **P<0.01, ***P<0.0001.

significant increase in CBs alignment defects and Tin-positive CB numbers in transheterozygous embryos, suggesting that *MSP300* and *WASp* function in a similar pathway during heart closure to regulate actin dynamics (Fig. 7E,F-H). Interestingly, removing WASp function had a negative impact on the localization of the ECM proteins LamA and Trol that was similar to that produced by *MSP300* and integrin complex loss of function (Fig. 6A‴-D‴), strengthening their involvement in the same mechanism.

To further confirm the link between F-actin and MSP300 localization, we performed Phalloidin staining to reveal the F-actin pattern in migrating CBs. Interestingly, F-actin accumulates on basal and apical sides of CBs, very much like CAP and MSP300 (Fig. 8A-A‴ and Fig. S2B-B‴). Hence, we tested whether MSP300 was required to stabilize F-actin accumulation at the interface of the nucleus and the CAP-Focal adhesion complex. Indeed, MSP300 loss of function induced a strong decrease in localized F-actin expression in CBs (arrowheads, Fig. 8B-D). Strikingly, this F-actin phenotype was stronger for Tin-positive CBs, as Svp-positive CBs still accumulated F-actin in MSP300 mutants (arrows, Fig. 8B,C), suggesting a specific function for MSP300 in Tin-positive CBs.

Consistent with its known function, *WASp*^{3} mutant embryos show a significant reduction of F-actin levels in a similar manner to that in *MSP300* mutant hearts (Fig. 8D). Taken together, these data suggest that CAP and MSP300 control the cell cycle exit and alignment of CBs by facilitating a F-actin linkage of the nucleus with the CB cell

Development (2021) 148, dev192146. doi:10.1242/dev.192146

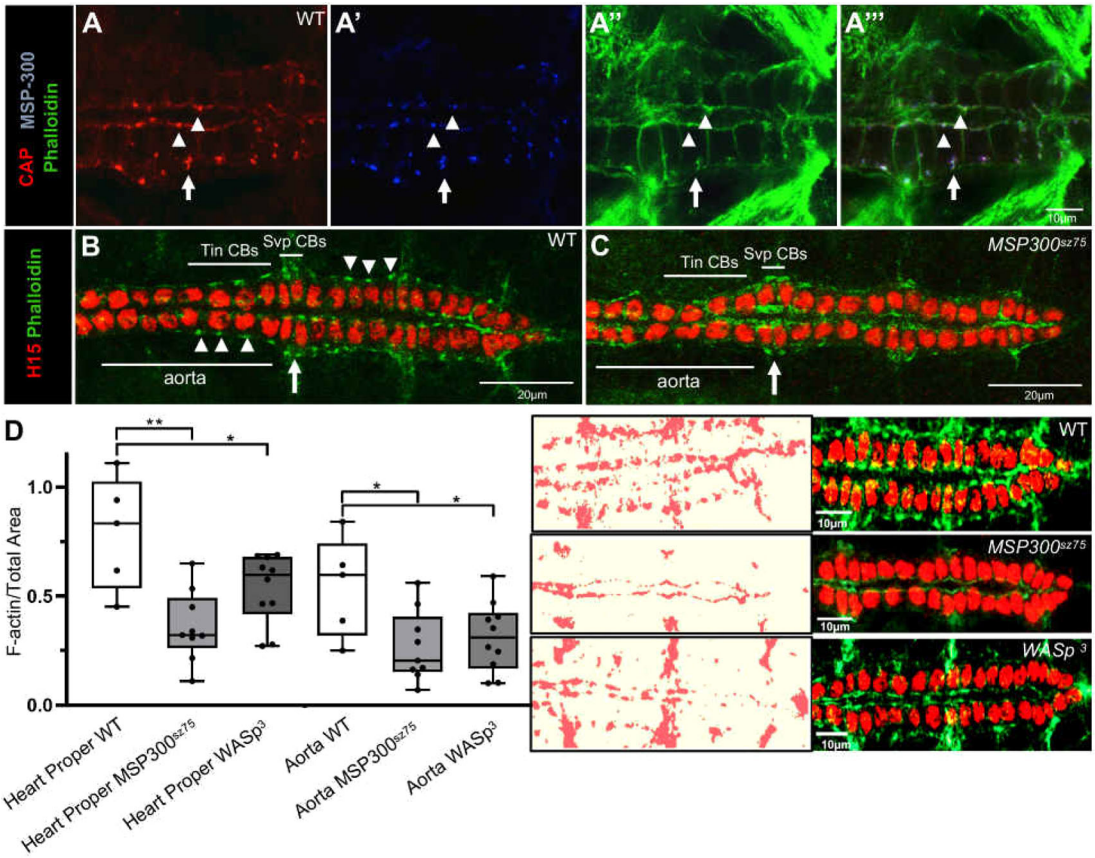

Fig. 8. CAP and MSP300 mediate F-actin bridging between the nucleus and integrin complex. (A-A‴) Dorsal view of the heart proper showing colocalization of CAP, MSP300 and F-actin on apical (arrowheads) and basal (arrows) sides of CBs, showing a polarized link between nucleus and cell membrane on each side of the cells. (B,C) Dorsal view of posterior part of the heart showing that loss of MSP300 (mildly affected embryo) leads to a decrease in F-actin polymerization, more particularly in Tin-positive CBs from aorta and heart proper (arrowheads). Arrows indicate that the F-actin level is similar in Svp-positive CBs in control and MSP300 mutant embryos. (D) F-actin quantification using the Weka segmentation tool in ImageJ in heart proper and aorta of wild-type, *MSP300*^{sz75} and *WASp*^{3} embryos. An unpaired two-tailed Wilcoxon-Mann-Whitney test demonstrates that the difference between control and both *MSP300* (heart proper, ***P*=0.0069; aorta, **P*=0.0289) and *WASp* mutants (heart proper, **P*=0.0359; aorta, **P*=0.0239) is statistically significant (wild type *n*=5; *MSP300*$^{-/-}$ *n*=9; *WASp*$^{-/-}$ *n*=10). The values of the box represent first and third quartile and the line represents the median. The whiskers represent the minimum and maximum of all the data. Right panels correspond to representative images of hearts stained using anti-H15 antibodies and with Phalloidin from the corresponding genotypes.

membrane. This function is limited during migration to the 'leading CB' population expressing Tin.

F-actin stress fibers have been shown to exert mechanical tension on the nucleus, providing mechano-sensing properties to orient the nucleus and modulate its shape during cell migration. Thus, we measured nucleus shape in *CAP* and *MSP300* mutants. We observed that *CAP* and *MSP300* null mutants or cardiac-specific CAP knockdown induce a significant decrease of nuclei volume as well as an increase in flatness relative to controls (Fig. 9A,B). Consistent with our findings, *WASp*^{3} mutant embryos show the same effect on nuclei shape, suggesting the requirement of actin stress fibers to maintain nuclei morphology during CBs migration.

DISCUSSION

In this study, we have analyzed expression and function of two novel regulators of cardiac morphogenesis: CAP, an integrin complex adaptor protein; and MSP300, a Nesprin protein belonging to the LINC complex. Our study highlights a crucial role for CAP and MSP300 in maintaining the nucleus-cell membrane connection via the integrin/vinculin adhesion complex, which is ultimately required in locking cell division processes during the migration progression of Tin-positive cardiomyocytes. (Fig. 8C). We also provide evidence that this nucleus-cytoskeleton-cell membrane link is important for maintaining CB polarity, contact between ipsilateral and contralateral CBs, and proper nucleus shape.

These mechanisms appear to be coupled and more work will be needed to determine whether the quiescent stage exit is a cause or a consequence of polarity and alignment defects. Slit localization is also affected in *MSP300* and *CAP* mutants, suggesting that Slit-mediated directionality of CB migration might be affected. Indeed, a conserved aspect of Slit/Robo signaling is its involvement in cell guidance mechanisms (Fish et al., 2011; Raza and Jacobs, 2016; Wu et al., 1999). In *Drosophila*, Slit is known to interact genetically with several members of the integrin complex (αPS3, βPS), and the integrins are required for apical localization of Slit and leading-edge activity. The direct coupling between the cell membrane and the ECM at integrin-based adhesion sites (focal adhesion) allows cells to mechanically sense their physical environment and tune downstream signaling events that regulate the organization of the cytoskeleton. Vinculin is a key player in focal adhesion, where it interacts directly with Talin and ensures a link between adhesion proteins and actin cytoskeleton (Burridge and Mangeat, 1984; Humphries et al., 2007; Rothenberg et al., 2018). In vertebrates and

Development (2021) 148, dev192146. doi:10.1242/dev.192146

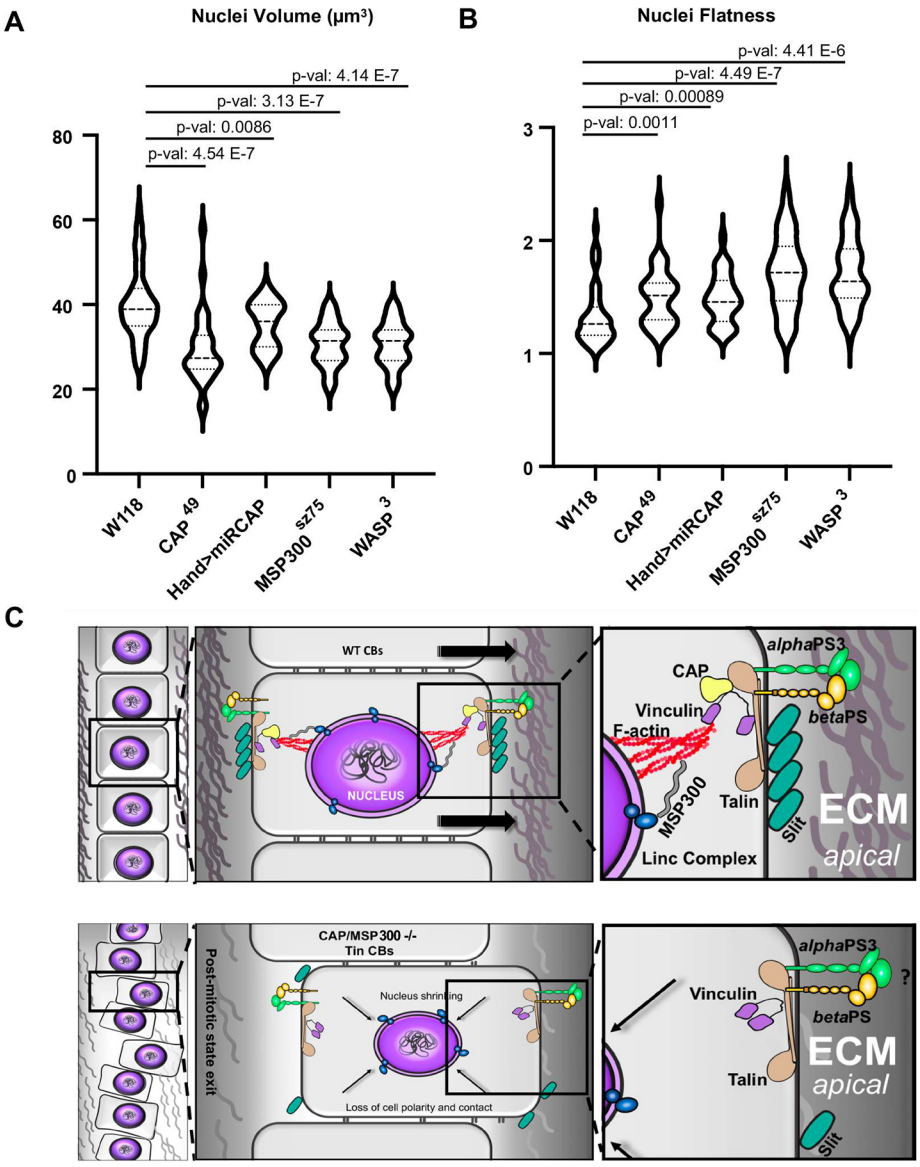

Fig. 9. CAP, MSP300 and WASp maintain CB nuclei morphology. (A,B) Nuclei morphology parameter assessment using nucleus J software in different genetic contexts. Nuclei volume is significantly reduced in *CAP*, *MSP300* and *WASp* mutant CBs, and by cardiac-specific knockdown of *CAP*. In contrast, the flatness of CB nuclei increases in the same genotypes compared with W118 control. Two tailed *P*-value was calculated using an unpaired Wilcoxon-Mann-Whitney test (wild type n=84, CAP^{49e} n=32, Hand>miRCAP n=32, $MSP300^{sz75}$ n=47, $WASp^{3}$ n=77). (C) Model of the nucleus-cytoskeleton-focal adhesion complex involving CAP adapter protein and the Nesprin protein MSP300 (top) with stable nuclei morphology and a polarized link to the cell membrane on apical and basal sides. Loss of *CAP* or *MSP300* (bottom) causes the loss of the Vinculin interaction with F-actin, leading to a weakening of focal adhesion and affecting Slit polarization. These defects, in turn, induce exit from the post-mitotic state, a decrease in cell-cell contacts between neighboring CBs and misalignment within the migrating CB rows. An impact on nuclei morphology is also observed.

in *Drosophila*, CAP has the potential to directly interact with Vinculin (Bharadwaj et al., 2013). In CBs, loss of Vinculin leads to disorganized CAP and irregular MSP300 localization, probably owing to the loss of Vinc-anchoring points at the cell membrane, resulting in changes in the number, polarity and motility of affected CBs. We propose that MSP300 and CAP ensure the connection of nuclei to adhesion complex via actin cytoskeleton and Vinculin, and could thus modulate the coordination between cell division arrest and the initiation of migration. However, even though both rows of CBs appear to reach the dorsal midline in *CAP* and *MSP300* mutant embryos, their expression pattern, which is maintained throughout cardiac tube formation, could suggest a potential secondary function in the fine regulation of the dynamics of CB migration.

MSP300 possesses spectrin repeats, allowing interaction with actin. In this study, we demonstrate the genetic interaction of *MSP300* with *CAP* and *WASp*, an activator of the Arp2/3 complex, suggesting that the branched actin network is involved in connecting the nucleus to the cell membrane (Padrick et al., 2011).

Transition from cell cycle exit to cell migration is a coordinated process that requires multilevel controls in terms of cell polarity, cell adhesion and differentiation involving changes in gene expression programs. LINC complexes are known to be important in transmitting mechanical stresses from the cytoskeleton to the inside of the nucleus that ultimately lead to changes in nuclear structure and organization, and to regulation of cell cycle progression (Uroz et al., 2018). Recently, the LINC complex has been shown to transmit the forces from the β1-integrin-engaged actin network to the nuclear lamina to directly regulate the expression of epidermal differentiation genes (Carley et al., 2021). Our results support these views, although the outcome might depend on the context. One of our interesting observations is that CAP-MSP300 dots accumulate at both sides of migrating CBs. Recent evidence suggests the existence of an actin structure called a perinuclear actin-cap that interacts with specific actin-cap-associated focal adhesion components at two positions in the direction of the aligned actin-cap fibers: at the leading lamellipodial edge and at the trailing edge of the cell. This newly identified actin structure is linked to the nucleus via the LINC complex (Kim et al., 2012; Maninova et al., 2017) and might be necessary for coordinating quiescence, cell polarity and nucleus shape during migration. Furthermore, nuclei deformations observed in *CAP*, *MSP300* and *WASp* mutant nuclei are reminiscent of a previously

Development (2021) 148, dev192146. doi:10.1242/dev.192146

described model based on results obtained after Nesprin 1 siRNA treatment of endothelial cells (Anno et al., 2012). Indeed, as in Nesprin 1 knockdown, CB nuclei seem more sensitive to deformation, and become smaller and flattened, suggesting that wild-type nuclei might be subjected to directional tensile forces along the apical-basal axis during CB migration.

Additional work will determine whether F-actin bound to the nucleus through MSP300 and to focal adhesions leads to a sustainable force transmission to CB nuclei and whether direct transmission of mechanical force to the nucleus can influence the exit of CBs from the cell cycle. Recent findings have shown that *nesprin-1* mutations lead to increased activation of the ERK pathway in mouse heart tissue (Zhou et al., 2017). In vertebrates, CAP/Ponsin has been also shown to repress the MAPK pathway (Zhang et al., 2006). In *Drosophila*, late EGFR-mediated ERK activation has been shown to promote a Tin-positive CB subpopulation (Schwarz et al., 2018). According to our data, one hypothesis is that CAP and MSP300 would contribute to the maintenance of the correct number of Tin-positive migrating CBs by counteracting the EGF pathway. Further investigations will be needed to clarify the involvement of CAP, F-actin and MSP300 in controlling these processes.

Our physiological analysis of *MSP300* mutant adult hearts indicate that the cardiac contractile function is affected. Fractional shortening in adults were strongly affected by *MSP300* knockdown and was linked to locally defective morphology of adult hearts.

During the publication process, a new study has shown that a similar phenotype occurs after CAP mutation in larvae and adult heart (Jammrath et al., 2020), suggesting that the MSP300-CAP connection might be conserved for the correct architecture and function in the adult heart. These preliminary results open new perspectives concerning the possible implication of this connection in the formation of the primitive cardiac tube of vertebrates.

MATERIALS AND METHODS

Drosophila genetics

The *Drosophila CAP* deletion mutant *dCAP49e* has a deleted 2.9 kb region downstream of the CAP^{CA06924} P-element. The *dCAP49e* mutant and *UAS-CAPmiR* construct were generated according to Bharadwaj et al. (2013). *dCAP49e* and *P(UAS-CAP.miRNA)3* were from the Bloomington Stock Center. The *MSP300*^{SZ75} mutant was a gift from Talila Volk (Weizmann Institute of Science, Rehovot, Israel). It carries truncation of the C-terminal region of MSP300 (Rosenberg-Hasson et al., 1996). MSP300 TRIP lines (32377 and 32848) myospheroid TRIP lines (27735 and 33642), WASp TRIP lines (25955 and 36647), a *scb*^{01288} mutant line (11035) and a EGFP-MSP300 protein trap (59757) were from the Bloomington Stock Center. Vinculin RNAi lines (v34585 and v34586; Kaushik et al., 2015) were obtained from the Vienna *Drosophila* Research Center. The Vinculin-GFP line is tagged at its N-terminus with superfolded GFP using a pFlyFos025866 Fosmid that encompasses the 8 kb of Vinculin gene along with 23.4 kb upstream and 6.8 kb downstream regions integrated in the attp2 site (Kale et al., 2018). Cardiac GAL4 drivers used in this study are Hand$^{4.2}$ and TinC Δ4.

Immunostaining

Drosophila embryos were processed for immunostaining as described previously for most of the experiments (Patel, 1994). Heat fixation were also performed on wild-type dechorionated embryos for 10 s in boiling water followed by a 5 min devitellinization in a 1:1 mix of heptan and methanol on a shaker. Microscopic observations were performed by confocal microscopy to produce images using Leica SP8. All images were acquired using a 40× oil objective with a numerical aperture of 1.3. The following antibodies were used: rabbit anti-CAP 1:1000 (a gift from A. L. Kolodkin, Johns Hopkins University School of Medicine, Baltimore, MD, USA; Bharadwaj et al., 2013), rabbit anti-Mef2 1:1000 (a gift from M. V. Taylor, School of Biosciences, Cardiff University, Cardiff, UK), guinea pig anti-MSP300 1:2000 (Rosenberg-Hasson et al., 1996) and guinea pig anti-Laminin A 1:1000 (a gift from T. Volk, Weizmann Institute of Science, Rehovot, Israel), guinea pig anti-H15 1:2000 (a gift from J. B. Skeath, Washington University School of Medicine, St Louis, MO, USA), rabbit anti-Trol 1:1000 (a gift from S. Baumgartner Lund University, Lund, Sweden), mouse anti-Slit at 1:100 (DSHB), anti-Seven up at 1:100 (DSHB), anti-Armadillo at 1:100 (DSHB), anti-α-Spectrin 1:100 (DSHB), anti-Vinculin 1:50 (Santa Cruz N-19) and Alexa fluor 488 Phalloidin 1:300 (Invitrogen A12379).

Optical cross-section of *Drosophila* embryonic heart tubes

IMARIS software 7.6.5 has been used to open images in a 2D display mode (Slice view). In the menu bar, we selected 'Edit – Crop 3D'. A rectangle, with yellow borders, will overlay on all three views. It represents the region of interest and it can be modified in size and position, resulting in the cross-sections of the selected part of the heart tube.

The Surpass mode is used to create a 3D reconstruction of the *Drosophila* embryonic heart tubes; setting the pointer on Navigate mode allows the resulting object to be rotated through a range of angles. This was carried out in two different regions: aorta and the heart proper.

Drosophila heart physiology

Semi-intact preparations of the fly hearts were made as described previously (Vogler and Ocorr, 2009). Female flies are used for technical reasons (females are bigger). Briefly, flies (20 each genotype) were dissected in oxygenated artificial hemolymph (AHL) to expose the linear tube-like heart. After a 15-20 min recovery in fresh oxygenated AHL, 30 s high-speed movies (~140 fps) of contracting hearts were captured with a 10× immersion objective. These movies were analyzed with the SOHA software (sohasoftware.com; Ocorr et al., 2007; Vogler and Ocorr, 2009; Fink et al., 2009). The following key heart function parameters were measured: diastolic interval (DI), systolic interval (SI), diastolic diameter (DD) and systolic diameter (SD). Functional parameters were calculated based on these measures including heart period (HP, DI+SI). Fractional shortening (FS) as a measure of contractility was calculated as FS=[(EDD−ESD)/EDD], where EDD is the DD and ESD is the SD.

F-actin quantification

F-actin was detected and quantified using the Weka segmentation tool in ImageJ in both heart proper and aorta in each embryo. The same classifier has been used on every image. The values are normalized to the total area of the heart.

Nuclei morphology measurement

Microscopic observations were performed by confocal microscopy to produce images using Leica SP8. All images were acquired using a 40× oil objective with a numerical aperture of 1.3, a pixel size of 0.054 µm (x,y) and voxel depth of 0.2 µm. Furthermore, all initial anisotropic voxels are converted to an isotropic voxel (i.e. cubic, xyz=0.1 µm) prior to calculation. The ImageJ plug-in NucleusJ was used to characterize nuclear morphology (Dubos et al., 2020; Poulet et al., 2015). A detailed description of the quantitative parameters generated by NucleusJ can be found in Poulet et al. (2015).

Quantification and statistical analysis

Statistical analyses were performed using Xlstat. The significance of the difference was determined using an unpaired Wilcoxon-Mann-Whitney test. All P-values are two tailed. P<0.05 was considered significant.

Acknowledgements

We thank Sophie Desset, Tristan Dubos and Caroline Vachias (the GReD institute) for their technical assistance, as well as CLIC facility.

Competing interests

The authors declare no competing or financial interests.

Author contributions

Conceptualization: G.J.; Methodology: B.B., J.-P.D.P., G.J.; Validation: C.D.; Formal analysis: C.D., G.J.; Investigation: C.D., G.J.; Resources: C.D., B.B.; Data curation: C.D., G.J.; Writing - original draft: G.J.; Writing - review & editing: K.J., G.J.; Visualization: I.W.; Supervision: G.J.; Project administration: G.J.; Funding acquisition: G.J.

Funding

This work was supported by the Agence Nationale de la Recherche Jeune Chercheur (JC) (CARDIAC-SPE) through FEDER/Region Auvergne Young Researcher, TEFOR-ANR Infrastructure and CAP-2025 ISITE challenge-3 grants.

References

Anno, T., Sakamoto, N. and Sato, M. (2012). Role of nesprin-1 in nuclear deformation in endothelial cells under static and uniaxial stretching conditions. *Biochem. Biophys. Res. Commun.* **424**, 94-99. doi:10.1016/j.bbrc.2012.06.073

Banerjee, I., Zhang, J., Moore-Morris, T., Pfeiffer, E., Buchholz, K. S., Liu, A., Ouyang, K., Stroud, M. J., Gerace, L., Evans, S. M. et al. (2014). Targeted ablation of nesprin 1 and nesprin 2 from murine myocardium results in cardiomyopathy, altered nuclear morphology and inhibition of the biomechanical gene response. *PLoS Genet.* **10**, e1004114. doi:10.1371/journal.pgen.1004114

Bharadwaj, R., Roy, M., Ohyama, T., Sivan-Loukianova, E., Delannoy, M., Lloyd, T. E., Zlatic, M., Eberl, D. F. and Kolodkin, A. L. (2013). Cbl-associated protein regulates assembly and function of two tension-sensing structures in Drosophila. *Development* **140**, 627-638. doi:10.1242/dev.085100

Biersmith, B., Wang, Z. H. and Geisbrecht, E. R. (2015). Fine-tuning of the actin cytoskeleton and cell adhesion during Drosophila development by the unconventional guanine nucleotide exchange factors myoblast city and sponge. *Genetics* **200**, 551-567. doi:10.1534/genetics.115.177063

Bryantsev, A. L. and Cripps, R. M. (2009). Cardiac gene regulatory networks in Drosophila. *Biochim. Biophys. Acta* **1789**, 343-353. doi:10.1016/j.bbagrm.2008.09.002

Burridge, K. and Mangeat, P. (1984). An interaction between vinculin and talin. *Nature* **308**, 744-746. doi:10.1038/308744a0

Busser, B. W., Haimovich, J., Huang, D., Ovcharenko, I. and Michelson, A. M. (2015). Enhancer modeling uncovers transcriptional signatures of individual cardiac cell states in Drosophila. *Nucleic Acids Res.* **43**, 1726-1739. doi:10.1093/nar/gkv011

Carley, E., Stewart, R. M., Zieman, A., Jalilian, I., King, D. E., Zubek, A., Lin, S., Horsley, V. and King, M. C. (2021). The LINC complex transmits integrin-dependent tension to the nuclear lamina and represses epidermal differentiation. *eLife* **10**, e58541. doi:10.7554/eLife.58541

Dixon, D. M., Choi, J., El-Ghazali, A., Park, S. Y., Roos, K. P., Jordan, M. C., Fishbein, M. C., Comai, L. and Reddy, S. (2015). Loss of muscleblind-like 1 results in cardiac pathology and persistence of embryonic splice isoforms. *Sci. Rep.* **5**, 9042. doi:10.1038/srep09042

Dubos, T., Poulet, A., Gonthier-Gueret, C., Mougeot, G., Vanrobays, E., Li, Y., Tutois, S., Pery, E., Chausse, F., Probst, A. V. et al. (2020). Automated 3D bio-imaging analysis of nuclear organization by NucleusJ 2.0. *Nucleus* **11**, 315-329. doi:10.1080/19491034.2020.1845012

Fink, M., Callol-Massot, C., Chu, A., Ruiz-Lozano, P., Belmonte, J. C. I., Giles, W., Bodmer, R. and Ocorr, K. (2009). A new method for detection and quantification of heartbeat parameters in Drosophila, zebrafish, and embryonic mouse hearts. *BioTechniques* **46**, 101-113. doi:10.2144/000113078

Fish, J. E., Wythe, J. D., Xiao, T., Bruneau, B. G., Stainier, D. Y., Srivastava, D. and Woo, S. (2011). A Slit/miR-218/Robo regulatory loop is required during heart tube formation in zebrafish. *Development* **138**, 1409-1419. doi:10.1242/dev.060046

Friedl, P., Wolf, K. and Lammerding, J. (2011). Nuclear mechanics during cell migration. *Curr. Opin. Cell Biol.* **23**, 55-64. doi:10.1016/j.ceb.2010.10.015

Fruleux, A. and Hawkins, R. J. (2016). Physical role for the nucleus in cell migration. *Journal of Physics. Condensed Matter* **28**, 363002. doi:10.1088/0953-8984/28/36/363002

Haack, T., Schneider, M., Schwendele, B. and Renault, A. D. (2014). Drosophila heart cell movement to the midline occurs through both cell autonomous migration and dorsal closure. *Dev. Biol.* **396**, 169-182. doi:10.1016/j.ydbio.2014.08.033

Haag, T. A., Haag, N. P., Lekven, A. C. and Hartenstein, V. (1999). The role of cell adhesion molecules in Drosophila heart morphogenesis: faint sausage, shotgun/DE-cadherin, and laminin A are required for discrete stages in heart development. *Dev. Biol.* **208**, 56-69. doi:10.1006/dbio.1998.9188

Hong, S.-E., Song, H. K. and Kim, D. H. (2014). Identification of tissue-enriched novel transcripts and novel exons in mice. *BMC Genomics* **15**, 592. doi:10.1186/1471-2164-15-592

Humphries, J. D., Wang, P., Streuli, C., Geiger, B., Humphries, M. J. and Ballestrem, C. (2007). Vinculin controls focal adhesion formation by direct interactions with talin and actin. *J. Cell. Biol.* **179**, 1043-1057. doi:10.1083/jcb.200703036

Ichikawa, T., Kita, M., Matsui, T. S., Nagasato, A. I., Araki, T., Chiang, S. H., Sezaki, T., Kimura, Y., Ueda, K., Deguchi, S. et al. (2017). Vinexin family (SORBS) proteins play different roles in stiffness-sensing and contractile force generation. *J. Cell Sci.* **130**, 3517-3531. doi:10.1242/jcs.200691

Jammrath, J., Reim, I. and Saumweber, H. (2020). Cbl-associated protein CAP contributes to correct formation and robust function of the Drosophila heart tube. *PLoS ONE* **15**, e0233719. doi:10.1371/journal.pone.0233719

Jin, H., Stojnic, R., Adryan, B., Ozdemir, A., Stathopoulos, A. and Frasch, M. (2013). Genome-wide screens for in vivo Tinman binding sites identify cardiac enhancers with diverse functional architectures. *PLoS Genet.* **9**, e1003195. doi:10.1371/journal.pgen.1003195

Junion, G., Spivakov, M., Girardot, C., Braun, M., Gustafson, E. H., Birney, E. and Furlong, E. E. M. (2012). A transcription factor collective defines cardiac cell fate and reflects lineage history. *Cell* **148**, 473-486. doi:10.1016/j.cell.2012.01.030

Kale, G. R., Yang, X., Philippe, J.-M., Mani, M., Lenne, P.-F. and Lecuit, T. (2018). Distinct contributions of tensile and shear stress on E-cadherin levels during morphogenesis. *Nat. Commun.* **9**, 5021. doi:10.1038/s41467-018-07448-8

Kaushik, G., Spenlehauer, A., Sessions, A. O., Trujillo, A. S., Fuhrmann, A., Fu, Z., Venkatraman, V., Pohl, D., Tuler, J., Wang, M. et al. (2015). Vinculin network-mediated cytoskeletal remodeling regulates contractile function in the aging heart. *Sci. Transl. Med.* **7**, 292-299. doi:10.1126/scitranslmed.aaa5843

Kim, D.-H., Khatau, S. B., Feng, Y., Walcott, S., Sun, S. X., Longmore, G. D. and Wirtz, D. (2012). Actin cap associated focal adhesions and their distinct role in cellular mechanosensing. *Sci. Rep.* **2**, 555. doi:10.1038/srep00555

Lovato, T. L. and Cripps, R. M. (2016). Regulatory networks that direct the development of specialized cell types in the Drosophila heart. *J. Cardiovasc. Dev. Dis.* **3**, 18. doi:10.3390/jcdd3020018

MacMullin, A. and Jacobs, J. R. (2006). Slit coordinates cardiac morphogenesis in Drosophila. *Dev. Biol.* **293**, 154-164. doi:10.1016/j.ydbio.2006.01.027

Maninova, M., Caslavsky, J. and Vomastek, T. (2017). The assembly and function of perinuclear actin cap in migrating cells. *Protoplasma* **254**, 1207-1218. doi:10.1007/s00709-017-1077-0

Medioni, C., Astier, M., Zmojdzian, M., Jagla, K. and Semeriva, M. (2008). Genetic control of cell morphogenesis during Drosophila melanogaster cardiac tube formation. *J. Cell Biol.* **182**, 249-261. doi:10.1083/jcb.200801100

Mellad, J. A., Waren, D. T. and Shanahan, C. M. (2011). Nesprins LINC the nucleus and cytoskeleton. *Current Opinion Cell Biology* **23**, 47-54. doi:10.1016/j.ceb.2010.11.006

Ocorr, K., Reeves, N. L., Wessells, R. J., Fink, M., Chen, H. S. V., Akasaka, T., Yasuda, S., Metzger, J. M., Giles, W., Posakony, J. W. et al. (2007). KCNQ potassium channel mutations cause cardiac arrhythmias in Drosophila that mimic the effects of aging. *Proc. Natl. Acad. Sci. USA* **104**, 3943-3948. doi:10.1073/pnas.0609278104

Padrick, S. B., Doolittle, L. K., Brautigam, C. A., King, D. S. and Rosen, M. K. (2011). Arp2/3 complex is bound and activated by two WASP proteins. *Proc. Natl. Acad. Sci. USA* **108**, 472-479. doi:10.1073/pnas.1100236108

Patel, N. H. (1994). Imaging neuronal subsets and other cell types in whole-mount Drosophila embryos and larvae using antibody probes. *Methods Cell Biol.* **44**, 445-487. doi:10.1016/S0091-679X(08)60927-9

Poulet, A., Arganda-Carreras, I., Legland, D., Probst, A. V., Andrey, P. and Tatout, C. (2015). NucleusJ: an ImageJ plugin for quantifying 3D images of interphase nuclei. *Bioinformatics* **31**, 1144-1146. doi:10.1093/bioinformatics/btu774

Puckelwartz, M. J., Kessler, E. J., Kim, G., Dewitt, M. M., Zhang, Y., Earley, J. U., Depreux, F. F., Holaska, J., Mewborn, S. K., Pytel, P. et al. (2010). Nesprin-1 mutations in human and murine cardiomyopathy. *J. Mol. Cell. Cardiol.* **48**, 600-608. doi:10.1016/j.yjmcc.2009.11.006

Qian, L., Liu, J. and Bodmer, R. (2005). Slit and Robo control cardiac cell polarity and morphogenesis. *Curr. Biol.* **15**, 2271-2278. doi:10.1016/j.cub.2005.10.037

Raza, Q. and Jacobs, J. R. (2016). Guidance signalling regulates leading edge behaviour during collective cell migration of cardiac cells in Drosophila. *Dev. Biol.* **419**, 285-297. doi:10.1016/j.ydbio.2016.09.005

Rosenberg-Hasson, Y., Renert-Pasca, M. and Volk, T. (1996). A Drosophila dystrophin-related protein, MSP-300, is required for embryonic muscle morphogenesis. *Mech. Dev.* **60**, 83-94. doi:10.1016/S0925-4773(96)00602-8

Rothenberg, K. E., Scott, D. W., Christoforou, N. and Hoffman, B. D. (2018). Vinculin force-sensitive dynamics at focal adhesions enable effective directed cell migration. *Biophys. J.* **114**, 1680-1694. doi:10.1016/j.bpj.2018.02.019

Rugendorff, A., Younossi-Hartenstein, A. and Hartenstein, V. (1994). Embryonic origin and differentiation of the Drosophila heart. *Roux's Arch. Dev. Biol.* **203**, 266-280. doi:10.1007/BF00360522

Santiago-Martinez, E., Soplop, N. H. and Kramer, S. G. (2006). Lateral positioning at the dorsal midline: slit and Roundabout receptors guide Drosophila heart cell migration. *Proc. Natl. Acad. Sci. USA* **103**, 12441-12446. doi:10.1073/pnas.0605284103

Schwarz, B., Hollfelder, D., Scharf, K., Hartmann, L. and Reim, I. (2018). Diversification of heart progenitor cells by EGF signaling and differential modulation of ETS protein activity. *eLife* **7**, e32847. doi:10.7554/eLife.32847

Stark, K. A., Yee, G. H., Roote, C. E., Williams, E. L., Zusman, S. and Hynes, R. O. (1997). A novel alpha integrin subunit associates with betaPS and functions in tissue morphogenesis and movement during Drosophila development. *Development* **124**, 4583-4594. doi:10.1242/dev.124.22.4583

Swope, D., Kramer, J., King, T. R., Cheng, Y.-S. and Kramer, S. G. (2014). Cdc42 is required in a genetically distinct subset of cardiac cells during Drosophila dorsal vessel closure. *Dev. Biol.* **392**, 221-232. doi:10.1016/j.ydbio.2014.05.024

Uroz, M., Wistorf, S., Serrra-Picamal, X., Conte, V., Sales-Pardo, M., Roca-Cusachs, P., Guimera, R. and Trepat, X. (2018). Regulation of cell-cycle progression by cell-cell and cell-matrix forces. *Nat. Cell Biol.* **20**, 646-654. doi:10.1038/s41556-018-0107-2

Vanderploeg, J. and Jacobs, J. R. (2015). Talin is required to position and expand the luminal domain of the Drosophila heart tube. *Dev. Biol.* **405**, 189-201. doi:10.1016/j.ydbio.2015.04.024

Vanderploeg, J., Vazquez Paz, L. L., MacMullin, A. and Jacobs, J. R. (2012). Integrins are required for cardioblast polarisation in Drosophila. *BMC Dev. Biol.* **12**, 8. doi:10.1186/1471-213X-12-8

Vogler, G. and Ocorr, K. (2009). Visualizing the beating heart in Drosophila. *J. Vis. Exp.* **31**, 1425. doi:10.3791/1425

Vogler, G., Liu, J., Iafe, T. W., Migh, E., Mihaly, J. and Bodmer, R. (2014). Cdc42 and formin activity control non-muscle myosin dynamics during Drosophila heart morphogenesis. *J. Cell Biol.* **206**, 909-922. doi:10.1083/jcb.201405075

Wang, J., Tao, Y., Reim, I., Gajewski, K., Frasch, M. and Schulz, R. A. (2005). Expression, regulation, and requirement of the toll transmembrane protein during dorsal vessel formation in Drosophila melanogaster. *Mol. Cell. Biol.* **25**, 4200-4210. doi:10.1128/MCB.25.10.4200-4210.2005

Wang, S., Reuveny, A. and Volk, T. (2015). Nesprin provides elastic properties to muscle nuclei by cooperating with spectraplakin and EB1. *J. Cell Biol.* **209**, 529-538. doi:10.1083/jcb.201408098

Wu, W., Wong, K., Chen, J., Jiang, Z., Dupuis, S., Wu, J. Y. and Rao, Y. (1999). Directional guidance of neuronal migration in the olfactory system by the protein Slit. *Nature* **400**, 331-336. doi:10.1038/22477

Zhang, M., Liu, J., Cheng, A., DeYoung, S. M., Chen, X., Dold, L. H. and Saltiel, A. R. (2006). CAP interacts with cytoskeletal proteins and regulates adhesion-mediated ERK activation and motility. *EMBO J.* **25**, 5284-5293. doi:10.1038/sj.emboj.7601406

Zhang, S., Amourda, C., Garfield, D. and Saunders, T. E. (2018). Selective filopodia adhesion ensures robust cell matching in the Drosophila heart. *Dev. Cell* **46**, 189-203. doi:10.1016/j.devcel.2018.06.015

Zhou, C., Li, C., Zhou, B., Sun, H., Koullourou, V., Holt, I., Puckelwartz, M. J., Warren, D. T., Hayward, R., Lin, Z. et al. (2017). Novel nesprin-1 mutations associated with dilated cardiomyopathy cause nuclear envelope disruption and defects in myogenesis. *Hum. Mol. Genet.* **26**, 2258-2276. doi:10.1093/hmg/ddx116

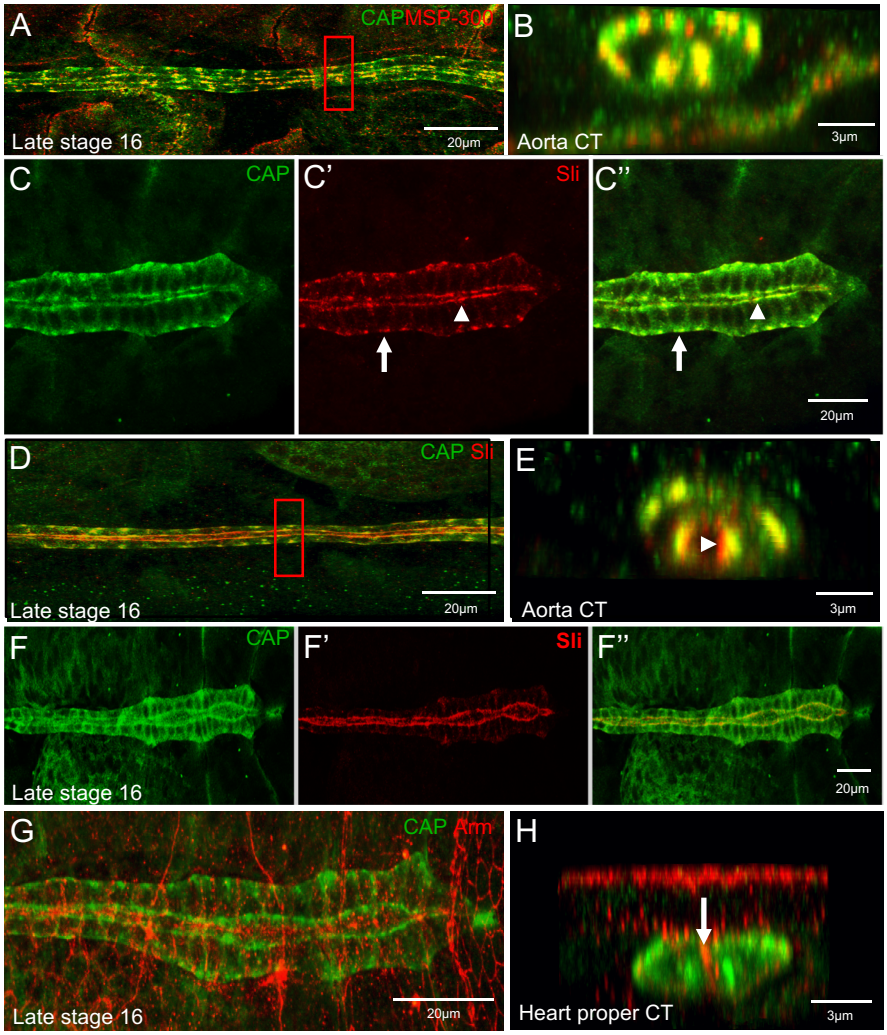

Fig. S1. CAP expression pattern in cardiac cells
(A, B) Dorsal view of a stage 16 embryo showing CAP and MSP300 localization in aorta and 3D reconstruction of transversal cut in aorta (B) validating accumulation of MSP300 and CAP on basal and apical side of CBs.
(C-C") Dorsal view of a stage 16 embryo showing that Slit colocalizes with CAP protein in a similar dotty pattern on apical (arrowheads) and basal sides of CBs (arrows).
(D, E) Dorsal view of a stage 16 embryo showing CAP and Slit localization in aorta and 3D reconstruction of transversal cut in aorta (E) validating accumulation of Slit and CAP on basal and apical side of CBs (arrowhead). Note that Slit protein is secreted at luminal side explaining the partial overlap with CAP.
(F-F") At late stage 16, Slit protein becomes accumulated at the lumen and strongly reduced at the basal side, while CAP is still maintained on both sides.
(G, H) CAP is not colocalized with Armadillo at the adherens junctions between contralateral CBs (arrow).

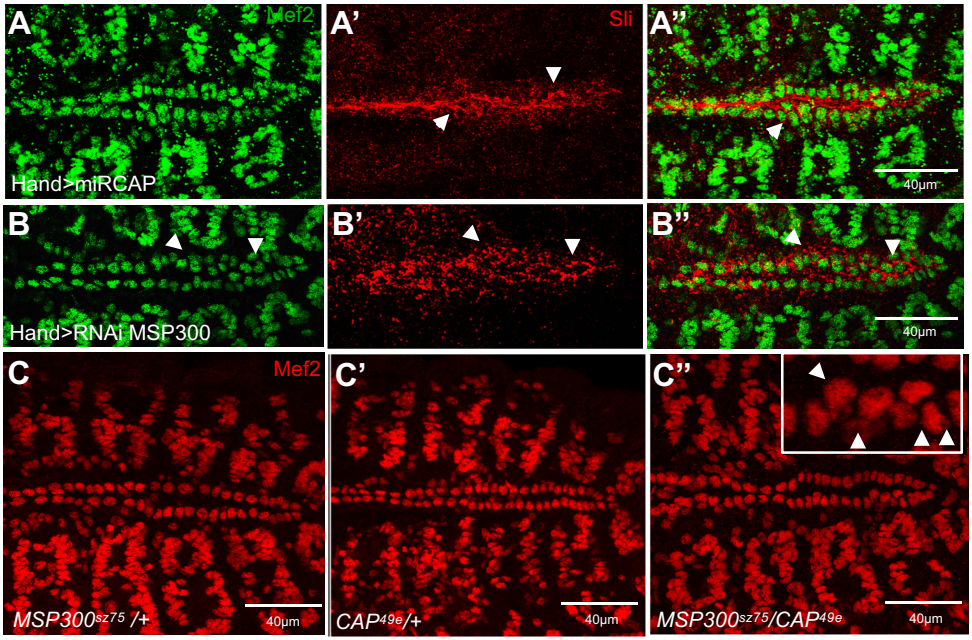

Fig. S2. CAP and MSP300 interact genetically to control CBs alignment and number (A-A") Cardiac specific miR KD of *CAP* using Hand-Gal4 driver induces CBs misalignment and polarity defects visualized with anti-Mef2 and anti-Slit antibodies (arrowheads) similarly to CAP and *MSP300* homozygous mutant. (B-B") Cardiac specific short hairpin KD (TRIP line) of MSP300 using Hand-Gal4 driver induces CBs misalignment and polarity defects visualized with anti-Mef2 and anti-Slit antibodies (arrowheads) similarly to *MSP300* homozygous mutant. (C-C") Immunostaining with anti-Mef2 in *CAP* and *MSP300* single heterozygous (C-C') by comparison with double heterozygous contexts (C"). No apparent change in CBs alignment can be observed in single heterozygous background while clusters of CBs in heart proper are visible in transheterozygous context (C", arrowheads in higher magnification window) demonstrating a genetic interaction between *CAP* and *MSP300* during CBs migration.

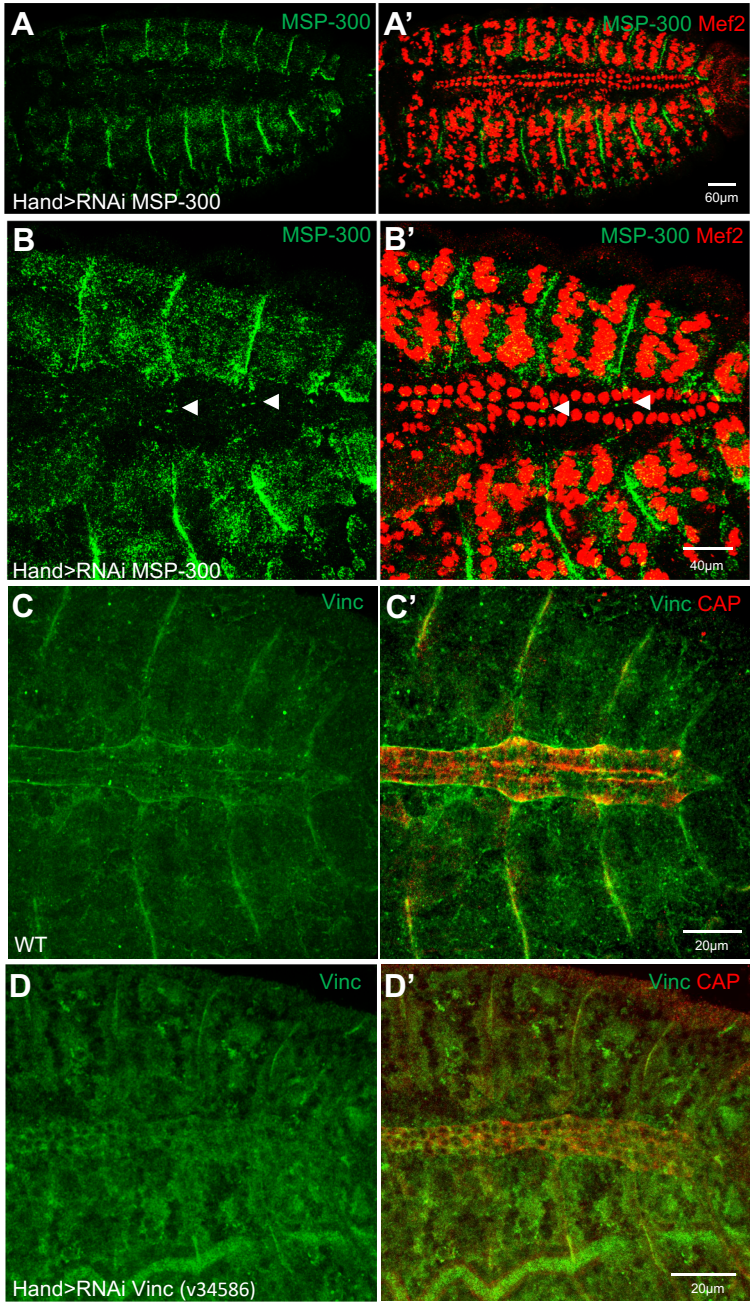

Fig. S3. Validation of RNAi lines targeting MSP300 and Vinc.
(A-B') Dorsal view of stage 16 embryo stained with anti-Mef2 and anti-MSP300 antibodies showing almost complete absence of MSP300 cardiac spots while in somatic muscles MSP300 is still highly present. Arrowheads in higher magnification pictures (B-B') point to remaining MSP300 accumulation.
(C-C') Dorsal view of stage 16 embryo stained with anti-CAP and anti-Vinc antibodies showing almost complete absence of Vinculin in RNAi context (D-D') compared to WT(C-C'). In both cases the HandGAL4 driver was used.

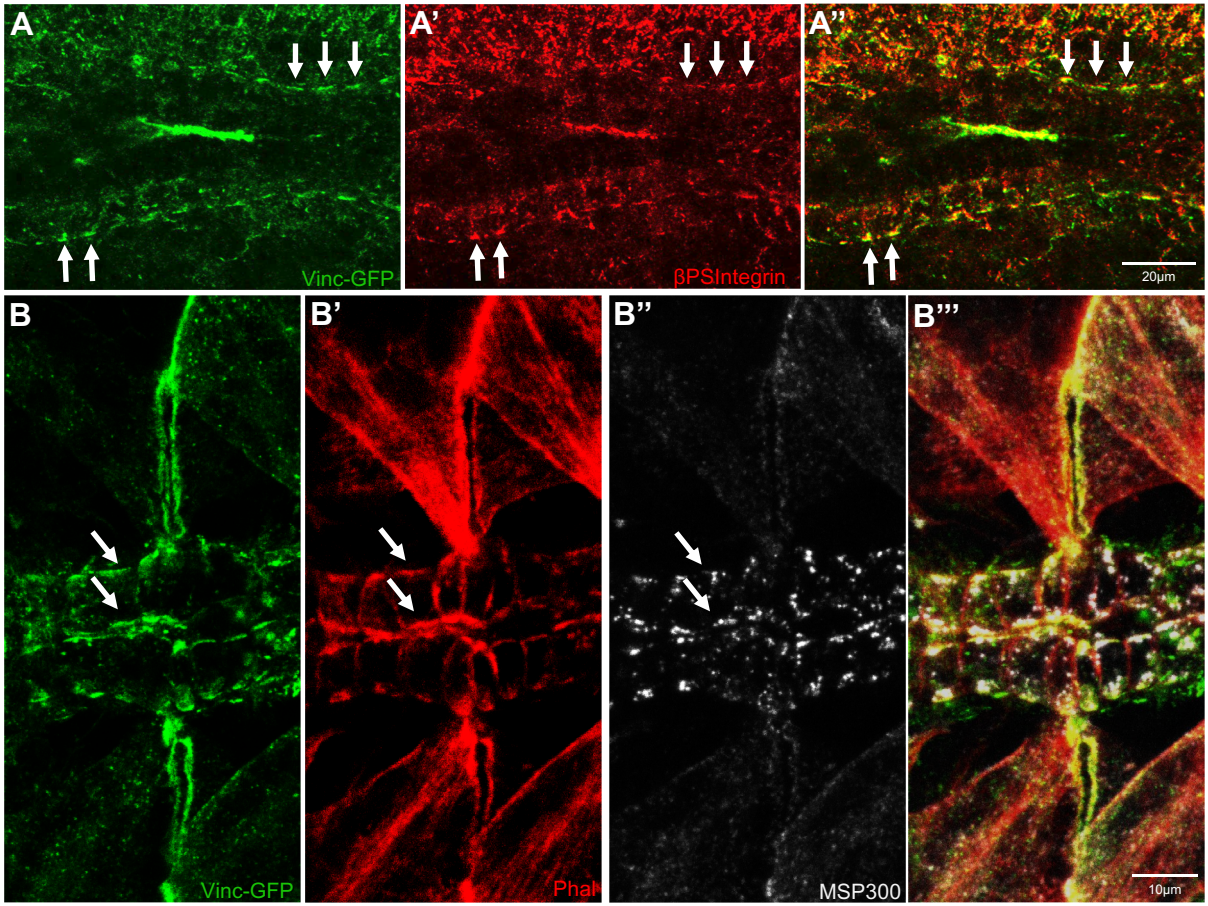

Fig. S4. Vinculin GFP colocalizes with βPS Integrin, F-actin and MSP-300
(A-A") Vinc-GFP colocalizes with bPS Integrin in cardioblasts (arrows) suggesting its involvement in Integrin focal adhesion complex. (B-B"') Dorsal view of stage 16 embryo showing Vinc-GFP colocalization with F-actin and MSP300 on apical and basal sides (arrows) suggesting a focal adhesion-based process connected to the nucleus through F-Actin.

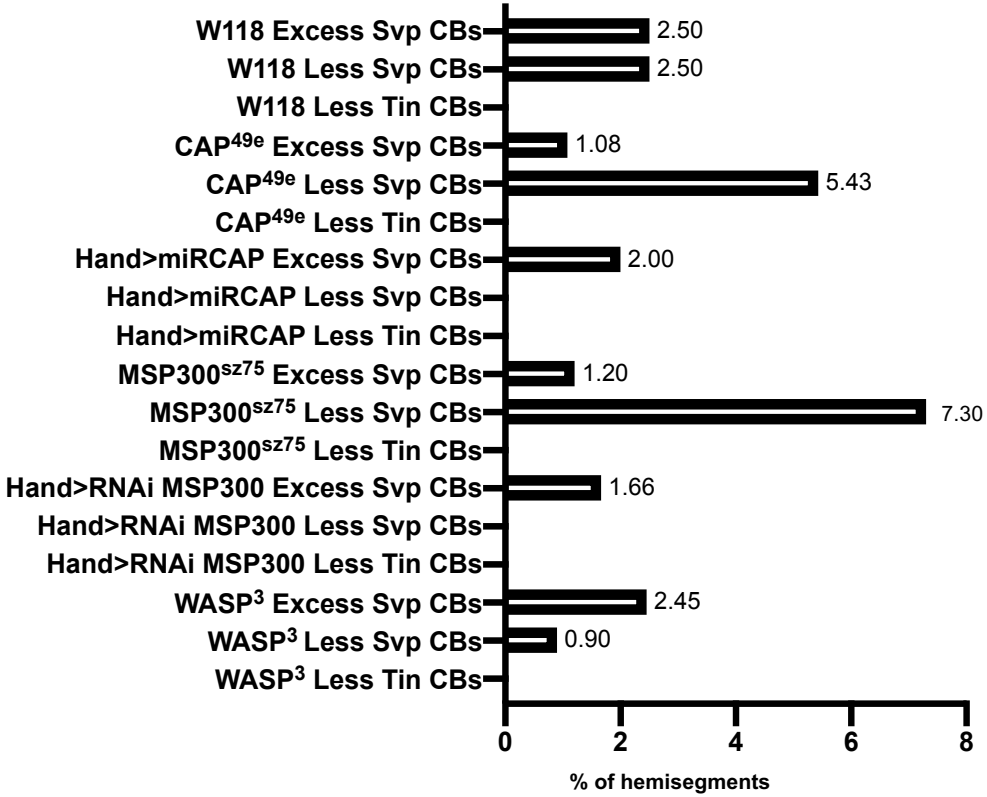

Fig. S5. Bar chart showing the percentage of hemi-segments with changes in CBs number other than an excess of Tin CBs

Data are represented as percentage of hemi-segment presenting either excess Svp +CBs, Less Svp+CBs or less Tin+CBs. (W118 n=240, *CAP49e* n=360, Hand>miRCAP n=240, *MSP300sz75* n=360, Hand>RNAi MSP300 n=240, *MSP300sz75/+* n= 240, *MSP300sz75/CAP49e* n=240, *WASp*^{3} n=240)